J Physiol 598.8 (2020) pp 1591–1609

The Journal of Physiology

Impaired muscle spindle function in murine models of muscular dystrophy

Laura Gerwin[1,2], Sarah Rossmanith[1], Corinna Haupt[1], Jürgen Schultheiß[1], Heinrich Brinkmeier[3], Reginald E. Bittner[4] and Stephan Kröger[1]

[1]*Department of Physiological Genomics, Biomedical Center, Ludwig-Maximilians-University, Großhaderner Str. 9, D-82152 Planegg-Martinsried, Germany*
[2]*Institute for Stem Cell Research, German Research Center for Environmental Health, Helmholtz Centre Munich, Ingolstädter Landstraße 1, D-85764 Neuherberg, Germany*
[3]*Institute for Pathophysiology, University Medicine Greifswald, Martin-Luther-Str. 6, 17489, Greifswald, Germany*
[4]*Neuromuscular Research Department, Center for Anatomy and Cell Biology, Medical University of Vienna, Waehringerstrasse 13, 1090 Vienna, Austria*

Edited by: Richard Carson & Dario Farina

Linked articles: This article is highlighted in a Perspectives article by Papaioannou & Dimitriou. To read this article, visit https://doi.org/10.1113/JP279611.

Key points

- Muscular dystrophy patients suffer from progressive degeneration of skeletal muscle fibres, sudden spontaneous falls, balance problems, as well as gait and posture abnormalities.
- Dystrophin- and dysferlin-deficient mice, models for different types of muscular dystrophy with different aetiology and molecular basis, were characterized to investigate if muscle spindle structure and function are impaired.
- The number and morphology of muscle spindles were unaltered in both dystrophic mouse lines but muscle spindle resting discharge and their responses to stretch were altered.
- In dystrophin-deficient muscle spindles, the expression of the paralogue utrophin was substantially upregulated, potentially compensating for the dystrophin deficiency.
- The results suggest that muscle spindles might contribute to the motor problems observed in patients with muscular dystrophy.

Abstract Muscular dystrophies comprise a heterogeneous group of hereditary diseases characterized by progressive degeneration of extrafusal muscle fibres as well as unstable gait and frequent falls. To investigate if muscle spindle function is impaired, we analysed their number, morphology and function in wildtype mice and in murine model systems for two distinct types of muscular dystrophy with very different disease aetiology, i.e. dystrophin- and dysferlin-deficient mice. The total number and the overall structure of muscle spindles in soleus muscles of both dystrophic mouse mutants appeared unchanged. Immunohistochemical analyses of wildtype muscle spindles revealed a concentration of dystrophin and β-dystroglycan in intrafusal fibres

Laura Gerwin obtained her MSc degree in biology with a specialization in medical biology at the Technical University of Munich, Germany. She then joined the Institute of Stem Cell Research at the Helmholtz Centre, Munich, the German Research Centre for Environmental Health, and worked in the group of Prof. Stephan Kröger to obtain her PhD at the Ludwig-Maximillians-University in Munich, Germany. She is interested in the communication between brain and muscles, specifically in the function of muscle spindles, and currently works as a manager for technology transfer at the Ludwig-Maximillians-University, Munich.

[The copyright line for this article was changed on 7 April 2020 after original online publication].

DOI: 10.1113/JP278563

outside the region of contact with the sensory neuron. While utrophin was absent from the central part of intrafusal fibres of wildtype mice, it was substantially upregulated in dystrophin-deficient mice. Single-unit extracellular recordings of sensory afferents from muscle spindles of the extensor digitorum longus muscle revealed that muscle spindles from both dystrophic mouse strains have an increased resting discharge and a higher action potential firing rate during sinusoidal vibrations, particularly at low frequencies. The response to ramp-and-hold stretches appeared unaltered compared to the respective wildtype mice. We observed no exacerbated functional changes in dystrophin and dysferlin double mutant mice compared to the single mutant animals. These results show alterations in muscle spindle afferent responses in both dystrophic mouse lines, which might cause an increased muscle tone, and might contribute to the unstable gait and frequent falls observed in patients with muscular dystrophy.

(Received 2 July 2019; accepted after revision 24 January 2020; first published online 31 January 2020)
Corresponding author S. Kröger: Department of Physiological Genomics, Biomedical Centre, Ludwig-Maximilians-University, Großhaderner Str. 9, D-82152 Planegg-Martinsried, Germany. Email: skroeger@lmu.de

Introduction

Muscular dystrophies (MDs) are a heterogeneous group of more than 30 different, mostly inherited diseases that are all characterized by peripheral muscle weakness and degeneration of the musculo-skeletal system (Mercuri & Muntoni, 2013). MD patients also suffer from postural instability and frequent falls (Hsu & Furumasu, 1993; Mahjneh *et al.* 2001; Pradhan *et al.* 2006), but the cause of these symptoms is unknown. The molecular basis of MDs are mutations that directly or indirectly affect the dystrophin-associated glycoprotein complex (DGC; Campbell & Kahl, 1989; Gao & McNally, 2015). The most common form of muscle dystrophy in humans is Duchenne muscular dystrophy (DMD; MIM #310200), which affects approximately 1 in 5000 boys (Mah *et al.* 2014), making it one of the most common recessive disorders in the human population. DMD is caused by mutations in the *DMD* gene, which codes for dystrophin (Waite *et al.* 2012). Dystrophin is a large cytoskeletal protein, which in skeletal muscle (via the DGC) provides a molecular link between subsarcolemmal F-actin filaments and the extracellular matrix (Blake & Kröger, 2000; Ervasti, 2007; Waite *et al.* 2012). This link mechanically stabilizes the sarcolemmal membrane, particularly during muscle contraction. Accordingly, mutations in dystrophin or in other proteins that directly or indirectly affect the DGC cause an interruption of this molecular link leading to mechanical lability of the sarcolemmal membrane and subsequent contraction-induced damage (Goldstein & McNally, 2010; Le Rumeur *et al.* 2010; Waite *et al.* 2012; Mercuri & Muntoni, 2013). Due to a number of mechanisms, including changes in the regenerative capacity of satellite cells (Chang *et al.* 2016) and loss of signalling capacity of the DGC (Constantin, 2014), over time regeneration cannot compensate for the degenerative loss of muscle tissue (Wallace & McNally, 2009). This ultimately leads to a reduction in muscle mass, loss of contractile force and, in the case of DMD, to premature death of the affected person due to respiratory or cardiac muscle failure (Mosqueira *et al.* 2013).

Dysferlinopathies (including limb girdle muscular dystrophy 2B; MIM #253601, and Miyoshi myopathy; MIM #254130) are another rare and clinically heterogeneous group of MDs also characterized by muscle weakness and wasting but with a completely different molecular cause and disease progression (Cardenas *et al.* 2016). The phenotype of this disease is much milder compared to DMD with an onset between the second and third decade (Rosales *et al.* 2010). A mutation in the *DYSF* gene on chromosome region 2p13 leads to a reduced function of dysferlin (Bashir *et al.* 1998; Liu *et al.* 1998; Aoki *et al.* 2001), a single-pass transmembrane protein with important roles during membrane fusion and trafficking (Anderson *et al.* 1999; Cardenas *et al.* 2016; Barthelemy *et al.* 2018). When microlesions in the plasma membrane occur, dysferlin-containing vesicles are recruited to the injury site in a Ca^{2+}-dependent manner (Han & Campbell, 2007; Matsuda *et al.* 2015) and dysferlin then appears to promote vesicle aggregation and fusion with the plasma membrane to reseal the injury site (McNeil, 2009). Accordingly, loss of dysferlin leads to an impaired membrane repair and subsequently to a degeneration of skeletal muscle fibres, causing muscle weakness. The functions of dysferlin in skeletal muscle fibres are not completely understood and additional functions of dysferlin, including an impaired Ca^{2+} homeostasis during mechanical stress (Kerr *et al.* 2013), might contribute to the degeneration of skeletal muscle tissue.

Coordinated movements, including locomotion, and their control, require proprioceptive information, i.e. information about muscle tone as well as position and movement of the extremities in space (Dietz, 2002; Proske & Gandevia, 2018). Muscle spindles are encapsulated primary proprioceptive sensory receptors. Muscle spindle sensory afferents inform the CNS about the extent

and speed of muscle lengthening (Proske & Gandevia, 2012; Blecher *et al.* 2018; Kröger, 2018). In adult mice, muscle spindles are 200–400 μm long and consist of 3–8 specialized intrafusal muscle fibres that lie in parallel with extrafusal muscle fibres (Banks, 1994; Bewick & Banks, 2015). The central (equatorial) part of intrafusal muscle fibres is innervated by two types of afferent proprioceptive sensory fibres (whose peripheral axons are termed 'type Ia afferents' and 'type II afferents' according to their axonal conduction velocity; Banks, 2015). The terminals of Ia afferents wrap around intrafusal fibres and form so-called annulospiral sensory nerve endings whereas those of type II afferents, when present, flank the Ia afferents (Schroder *et al.* 1989; Sonner *et al.* 2017). Type II afferents have so far not been detected in mice by immunohistochemical and electrophysiological methods (Wilkinson *et al.* 2012; Zhang *et al.* 2014, 2015; Gerwin *et al.* 2019). Proprioceptive sensory neurons generate action potentials with frequencies that are proportional to the size of the stretch and to the speed of stretching (De-Doncker *et al.* 2003). The cell bodies of these pseudounipolar sensory neurons constitute a minor fraction of all neurons in the dorsal root ganglion (DRG; Kashkoush *et al.* 2019) and their peripheral endings can be labelled by antibodies against the vesicular glutamate transporter 1 (VGluT1; Wu *et al.* 2004).

In addition to the sensory neurons, intrafusal muscle fibres are innervated by efferent γ-motoneurons (fusimotor innervation; Banks, 1994). Axons of γ-motoneurons enter the spindle together with the sensory fibres in the central region but innervate intrafusal muscle fibres exclusively at both ends (polar regions) where they form cholinergic synapses that appear functionally similar to neuromuscular junctions formed by γ-motoneurons on extrafusal muscle fibres. γ-Motoneurons modulate the sensitivity of muscle spindles by inducing contraction in the polar region of the intrafusal muscle fibres to exert tension on the equatorial region of the muscle fibre (Banks, 1994; Proske, 1997). This allows for continuous control of the mechanical sensitivity of spindles over the wide range of lengths and velocities that occur during normal motor behaviours.

Patients with MDs of the Duchenne type or with dysferlinopathies often experience sudden spontaneous falls, balance problems, as well as gait and posture abnormalities (Hsu & Furumasu, 1993; Mahjneh *et al.* 2001; Pradhan *et al.* 2006), suggesting that their proprioceptive system might be impaired. In agreement with this hypothesis, morphological changes in muscle spindles have been reported in dystrophic muscles from mice (Ovalle & Dow, 1986; Nahirney & Ovalle, 1993; Nahirney *et al.* 1997) and humans (Cazzato & Walton, 1968; Swash & Fox, 1976; Kararizou *et al.* 2007; Skuk *et al.* 2010). To investigate if muscle spindle function is also affected, we analysed the structure and molecular composition of muscle spindles in several mouse lines that carry mutations similar to mutations in humans with particular forms of MD and combined this analysis with electrophysiological recordings from single-unit muscle spindle afferents. The mouse lines analysed included the DMD^{mdx} mouse line (Bulfield *et al.* 1984), which harbours a non-sense mutation in exon 23 of the dystrophin gene, eliminating the expression of dystrophin in all tissues (Sicinski *et al.* 1989). This mouse is a widely used model system for DMD (Willmann *et al.* 2009). We also used the SJL-Dysf C57BL/6 mouse (*dysf*$^{-/-}$) a model system for dysferlinopathies (Bittner *et al.* 1999; Hornsey *et al.* 2013). Utrophin-deficient mice (*utrn*$^{-/-}$) have a very mild phenotype and only subtle changes in skeletal muscle tissue (Deconinck *et al.* 1997; Grady *et al.* 1997), and were included in the analysis as models for very mild forms of MD.

Our results show that muscle spindles from wildtype and dystrophic mice did not differ in the number, morphology and response to ramp-and-hold stretches. However, the action potential frequency at rest and the sensitivity to sinusoidal vibrations were increased in dystrophic muscles, demonstrating that muscle spindles from dystrophic mice have functional defects, which might contribute to the unstable gait and frequent falls observed in patients with MD.

Methods

Ethical approval

Use and care of animals was approved by German authorities and according to national law (§7 TierSchG). Animal procedures were performed according to the guidelines from Directive 2010/63/EU of the European Parliament on the protection of animals used for scientific purposes. All experiments were approved by the local authorities of the State of Bavaria, Germany (Az.: ROB-55.2-2532.Vet_02-17-82).

Animals

Male mice aged 10–15 weeks of 22–28 g from the following strains were used: C57BL/6J (Charles River Laboratories, Erkrath, Germany); C57BL/10Sc, C57BL/10ScSn/DMD^{mdx}/J (DMD^{mdx}; Bulfield *et al.* 1984; bred in the Department of Laboratory Animal Science of the Medical faculty at the University of Greifswald, Germany); C57BL/10Sc/Utro (*utrn*$^{-/-}$; Deconinck *et al.* 1997; Grady *et al.* 1997); SJL-Dysf C57BL/6 (*dysf*$^{-/-}$; Bittner *et al.* 1999); and DMD^{mdx}SJL-dysf C57BL/6 [DMD^{mdx}-*dysf*$^{-/-}$; maintained at the Division for Laboratory Animal Science and Genetics (Medical University Vienna, Himberg, Austria) under

institutionally approved protocols for the humane treatment of animals]. The DMD^{mdx}-*dysf*$^{-/-}$ mouse is a combination of the DMD^{mdx} and the *dysf*$^{-/-}$ mouse lines. This mouse model has a more severe dystrophic phenotype regarding skeletal muscle degeneration compared to either single-mutant animal (Lowe *et al.* 2006; Han *et al.* 2011). At most five adult animals were housed in a sterile cage on a 12-h light/dark cycle with *ad libitum* access to food and water. Experimental protocols were designed to the number of animals and were performed in Munich following protocols in compliance with the German law for animal protection. The authors declare that their work complies with the ethical principles under which *The Journal of Physiology* operates.

Immunofluorescence

Immunofluorescence labelling was performed as described previously (Zhang *et al.* 2014; Gerwin *et al.* 2019). To obtain muscle tissue for immunohistochemistry, mice were deeply anaesthetized via an I.P. injection of ketamine (100 mg kg^{-1}; Pfizer, Berlin, Germany) and xylazine (10 mg kg^{-1}; Bayer AG, Leverkusen, Germany). Depth of anaesthesia was assessed by the abolition of pedal reflexes. After transcardial perfusion with PBS followed by 4 % paraformaldehyde (PFA), the muscles were dissected. The distribution of the immunofluorescence signal was similar in soleus, quadriceps and EDL muscles. Muscles were post-fixed in 4% PFA for 2 h and then incubated in 30% sucrose in PBS overnight at 4°C. Fixed muscles were embedded in Tissue-Tek O.C.T. Compound (Sakura Finetek Europe, AJ Alphen an den Rijn, the Netherlands), rapidly frozen and cryo-sectioned along the longitudinal axis at 20–30 µm thickness and then air-dried.

Dried frozen sections were rehydrated for 10 min in PBS. In the case of anti-dysferlin antibodies, sections were incubated twice in 1 mg ml^{-1} sodium borohydrate for 4 min to reduce background immunofluorescence. Sections were then blocked in PBS containing 0.2% Triton X-100 (Sigma-Aldrich Chemie GmbH, Taufkirchen, Germany) and 1% bovine serum albumin (Carl Roth GmbH, Karlsruhe, Germany; blocking solution) for 30 min at room temperature and incubated with the primary antibody in blocking solution at 4°C overnight.

Sensory nerve terminals were stained using antibodies from guinea pig against vGluT1 (AB5905, Millipore, Darmstadt, Germany; 1:1000; Zhang *et al.* 2015; Gerwin *et al.* 2019). In addition, the following antibodies were used: mouse anti-utrophin (NCL-DRP2; Leica Biosystems, Nussloch, Germany; 1:4), rabbit anti-dysferlin (ab124684; Abcam, Cambridge, UK; 1:20), mouse anti-dysferlin (HAMLET-CE; Leica Biosystems; 1:50), mouse anti-β-dystroglycan (NCL-b-DG, Leica Biosystems; 1:75) and rabbit anti-dystrophin (RB-9024; ThermoFisher Scientific, Planegg, Germany; 1:100).

Primary antibodies were detected using the appropriate Alexa488- and Alexa594-conjugated goat anti-rabbit (A11037; Invitrogen; 1:1000), goat anti-mouse (A21125; Invitrogen; 1:1000) or donkey anti-guinea pig (AP1493SD; Millipore; 1:500) secondary antibody. Each of the secondary antibodies was preabsorbed against IgGs of the other two species, eliminating cross-reactivity in double-immunofluorescence analyses. No specific labelling was observed when the primary antibodies were omitted.

After immunofluorescence labelling, the sections were embedded in Mowiol mounting medium (Carl Roth) and analysed using a Zeiss LSM 710 laser scanning confocal microscope (Carl Zeiss AG, Oberkochen, Germany; Gerwin *et al.* 2019) or a SP8X WLL microscope (Leica, Wetzlar, Germany) at the Core-Facility Bioimaging of the Biomedical Centre. The LSM 710 was equipped with an argon laser (laser line 488 nm), a diode (laser line 405 nm), a DPSS laser (561 nm) and a HeNe laser (633 nm). Confocal z-stack images were generated using a 40× water immersion objective (LD C-Apochromat 40× with a numerical aperture of 1.1) and a multi-alkaline-based photomultiplier (PMT). Sequential recordings were performed to avoid bleed-through. The SP8X WLL microscope was equipped with a 405 nm laser, a WLL2 laser (470–670 nm) and an acousto-optical beam splitter. Sequentially scanned confocal Z-stacks of whole muscle spindles were obtained using 1 µm optical sections. Images were acquired with a 63× objective with a numerical aperture of 1.4 and an image pixel size of 80 nm. The following fluorescence settings were used: DAPI (4′,6-diamidino-2-phenylindole; excitation 405 nm; emission 410–470 nm), GFP (green fluorescent protein; excitation 489 nm; emission 492–550 nm), Cy3 (excitation 558 nm ; emission 560–600 nm) and Cy5 (excitation 650 nm ; emission 652–700 nm). GFP and Cy3 were recorded with hybrid photodetectors (HyDs), and DAPI and Cy5 with conventional photomultiplier tubes. Laser power levels, photomultiplier gain levels, scanning speed and confocal pinhole size were kept constant between experimental and control specimens. To avoid false positive results due to unspecific binding of antibodies, negative controls (without secondary antibodies) as well as sections of the corresponding mutated mouse were obtained in parallel. Digital processing of entire images, including adjustment of brightness and contrast, was performed using the Java image processing program software package Fiji (Schindelin *et al.* 2012). Compound images were assembled using CoreDraw (vs. 2017, Corel Corporation, Munich, Germany).

To determine the total number of muscle spindles in soleus muscles, entire muscles were cryosectioned along

the longitudinal axis at 20 μm thickness and stained with anti-vGluT1 antibodies and DAPI as described above. Each cryostat section was completely scanned by performing tile scans and all pictures from one section were aligned using the stitching tool to one complete image. This allowed the reconstruction and identification of all muscle spindles in an entire soleus muscle. Muscle spindles were identified by morphological criteria, i.e. positive immunofluorescence labelling of the annulospiral endings with anti-vGluT1 antibodies and the characteristic distribution of nuclei in nuclear chain and nuclear bag fibres. The number of muscle spindles was determined in three soleus muscles each from a different wildtype or mutant mouse line. Likewise, the number of circumferential elements of the annulospiral sensory nerve endings per 50 μm length of the intrafusal fibre was determined in the same set of sections by manual counting in soleus muscles from three different wildtype and dystrophic mice, respectively. Between 15 and 20 annulospiral endings per soleus muscle were analysed. Differences in the means of the total number of muscle spindles per soleus muscle and the mean of the number of circumferential segments were analysed using one-way ANOVA.

Muscle spindle electrophysiological response recordings

Afferent sensory neuron responses to stretch were assayed using an isolated muscle–nerve preparation previously described (Wilkinson *et al.* 2012; Franco *et al.* 2014; Gerwin *et al.* 2019). In brief, mice were killed by cervical dislocation to avoid any interference of the anaesthetic with the sensory afferent recordings. The extensor digitorum longus (EDL) muscle together with the deep peroneal branch of the sciatic nerve were then dissected and placed in a tissue bath containing oxygenated ACSF (Wilkinson *et al.* 2012). The tendons were sutured to a fixed post and on the other end to a lever arm, connected to a dual force and length controller (300C-LR, Aurora Scientific, Dublin, Ireland) allowing the simultaneous recording of muscle tension and muscle length. Sensory activity was sampled using a suction electrode (tip diameter 50–70 μm) which was connected to an extracellular amplifier (Model 1800, A&M Systems, Elkhart, IN, USA). Unless stated otherwise, at least five muscle spindles each from a different mouse were analysed. A signal was classified as being from a putative muscle spindle afferent if it displayed a characteristic instantaneous frequency response to stretch as well as a pause during twitch contraction (Wilkinson *et al.* 2012; Franco *et al.* 2014; Gerwin *et al.* 2019). Baseline muscle length (L_0) was defined as the minimal length at which maximal twitch contractile force was generated. For every muscle spindle afferent recording, a ramp-and-hold stretch (L_0 plus 7.5% of L_0; ramp speed 40% L_0 s^{-1}; ramp phase duration: 0.1 s; hold phase: 3.8 s; stretch duration: 4 s with 45 s intervals between each stretch), as well as 16 sinusoidal vibrations (peak-to-peak amplitudes: 5, 10, 50 and 100 μm, each with a frequency of 10, 25, 50 and 100 Hz for 9 s) were recorded. This series of recordings was repeated three times and represents a well-established protocol to assess murine muscle spindle function (Wilkinson *et al.* 2012; Franco *et al.* 2014; Gerwin *et al.* 2019). From these recordings the mean resting discharge (RD; average baseline firing rate) as well as the dynamic peak (DP; highest firing rate during ramp – baseline firing rate), the dynamic index (DI; dynamic peak – firing rate 0.45–0.55 s into stretch – baseline firing rate) and the static response (SR; firing rate 3.25–3.75 s into stretch – baseline firing rate) were determined (Wilkinson *et al.* 2012; Franco *et al.* 2014; Gerwin *et al.* 2019).

For analysis of the electrophysiological data, individual sensory neurons were identified by spike shape and interspike interval using the Spike Histogram feature of Lab Chart (AD Instruments, Sydney, Australia). The same program was used to determine the instantaneous firing frequency. Spindle afferent baseline firing rate, dynamic peak, dynamic index as well as the static stretch response were determined as described above. Up to three different muscle spindle afferents were recorded from one EDL muscle. Only recordings in which an individual muscle spindle afferent unit could be unambiguously identified were included in the analysis. Action potentials from additional muscle spindles that appeared during the stretch were not scored. No attempt was made to discriminate type Ia from type II afferents, because type II afferents have not been observed in mice (for detailed discussions see Wilkinson *et al.* 2012; Gerwin *et al.* 2019).

At the end of each recording, general muscle health was ensured by determining the maximal contractile force during a direct tetanic stimulation (500 ms train at 120 Hz frequency and 0.5 ms pulse length, supramaximal voltage; Grass SD9 stimulator; Natus, Pleasanton, CA, USA; Wilkinson *et al.* 2012; Gerwin *et al.* 2019). This value was normalized for differences in muscle size and mass by determining the diameter of the EDL muscle at L_0. With this information, the specific force (force/cross-sectional area) was determined in wildtype and dystrophic mice and compared to the previously reported peak force of the EDL of 23.466 N cm^{-2} (Larsson & Edstrom, 1986; Brooks & Faulkner, 1988). Consistent with the literature, we observed a small reduction of approximately 20% in the specific force of the EDL muscle from DMD^{mdx} compared to wildtype mice, but no difference between wildtype and $dysf^{-/-}$ mice (Horowits *et al.* 1990; Barton *et al.* 2010; Han *et al.* 2010; Hakim *et al.* 2011; Dillingham *et al.* 2015; Steinberger *et al.* 2015; Lloyd *et al.* 2019).

Statistical analysis of muscle spindle responses

Statistical analysis of the electrophysiological experiments was performed as previously described (Gerwin *et al.* 2019). Only single-unit spindle afferent responses that could be recorded without interruption throughout the entire experiment were included in the analysis. For the ramp and hold stretches, baseline values for all parameters (baseline firing rate, dynamic peak, dynamic index, and the static stretch response) were determined as an average of three stretches and the mean of all recordings was compared between wildtype and mutant mice. Values are reported as mean of the frequency (imp s^{-1}) in a dot plot with each dot representing a different muscle spindle response. Statistical significance was determined using one-way ANOVA with Dunnett's multiple comparisons test.

For the sinusoidal vibrations, the mean of the total number of action potentials per 9 s (imp 9 s^{-1}) for each of the four frequencies and four amplitudes was determined and the means were compared between wildtype and mutant mice. Data are shown as imp 9 s^{-1} in a dot plot with each dot representing an independent experiment. Statistical significance was determined using one-way ANOVA and Dunnett's multiple comparisons test. All analyses were performed using GraphPad Prism (v8; Graphpad Software, Inc., La Jolla, CA, USA). The level of significance (*P*-value) for all statistical tests was set at $^{*}< 0.05$, $^{**} < 0.01$, $^{***} < 0.001$ and $^{****}<0.0001$.

Results

Muscle spindle number and morphology is unaltered in dystrophic mice

To determine if muscle spindles are affected by the mutation in a similar way to extrafusal fibres in the surrounding muscle tissue, the total number and the overall structure of muscle spindles in the soleus muscle from wildtype, DMD^{mdx} and DMD^{mdx}-*dysf*$^{-/-}$ double mutant mice were determined. We chose the soleus muscle because the number of muscle spindles in this muscle has been extensively investigated and quantified (Lionikas *et al.* 2013; Sonner *et al.* 2017). To analyse the number of spindles per muscle, entire soleus muscles were cryosectioned and each section was stained with anti-vGluT1 antibodies. Each section was then tile-scanned and the fused tile images were analysed for the presence of muscle spindles (Fig. 1*A*). Manually counting the number of muscle spindles in dystrophic and wildtype mouse lines revealed an equal total number of approximately 10 muscle spindles per soleus muscle (Fig. 1*C*), which agrees well with the published number of 10–11 spindles per muscle in wildtype mice (Lionikas *et al.* 2013; Sonner *et al.* 2017). This result demonstrates that mutations in dystrophin and dysferlin did not affect the number of muscle spindles per soleus muscle.

To investigate if a loss of dystrophin affects the structure of the sensory nerve terminal, sections of the central parts of muscle spindles from three mice from each wildtype strain and three DMD^{mdx} mice were stained with anti-vGluT1 antibodies. The analysis was performed on the same set of muscle sections used to determine the total number of muscle spindles per soleus muscle. The number of circumferential segments of the sensory nerve terminal along segments of 50 µm of the intrafusal fibre was determined (red arrows in Fig. 1*B*). We observed an average of approximately 7.5 circumferential segments per 50 µm intrafusal fibre length in DMD^{mdx} as well as in both wildtype strains (Fig. 1*B* and *D*). Likewise, no obvious difference in the intensity and the distribution of the anti-vGluT1 labelling (Fig. 1*B*; see also Figs 2 and 3) between wildtype and DMD^{mdx} mice was observed, suggesting that the morphology of the annulospiral sensory nerve terminal was not apparently affected in dystrophic mice. In summary, our results suggest that the mutation in dystrophin or dysferlin did not overtly affect the overall structure or total number of muscle spindles in soleus muscles. This is in agreement with previous studies, which failed to identify structural changes in muscle spindles from dystrophic mice (Ovalle & Dow, 1986; Johnson & Ovalle, 1986; Nahirney & Ovalle, 1993; Nahirney *et al.* 1997).

Localization of different DGC components and of dysferlin in the central part of intrafusal fibres

To investigate the localization of different DGC components in the central region of intrafusal muscle fibres, sections of wildtype muscles were incubated with anti-vGluT1 antibodies to label the sensory nerve terminals. Spindles were additionally labelled with antibodies against dystrophin, β-dystroglycan or utrophin. High-resolution confocal microscopic analysis demonstrated an alternating non-overlapping immunofluorescence labelling pattern of dystrophin and vGluT1 in the central region of intrafusal fibres (Fig. 2*A*). Similar to what has been described previously (Nahirney & Ovalle, 1993), dystrophin was concentrated in the area of the intrafusal fibre plasma membrane, outside the contact region with the sensory nerve terminal, and appeared to be excluded from the area of direct intrafusal fibre to sensory nerve terminal contact. A similar mutually exclusive distribution along the intrafusal fibre was observed when wildtype muscle spindles were stained with antibodies against β-dystroglycan (Fig. 2*B*), suggesting that both components of the DGC co-distribute. The labelling pattern was similar in soleus, quadriceps and EDL muscle from wildtype mice. These results indicate that a DGC

containing dystrophin and β-dystroglycan is formed in the sarcolemma of intrafusal fibres in a particular subcellular region. Interestingly, utrophin was undetectable in the central (equatorial) region of C57BL/6 wildtype muscle spindles in all three muscles (Fig. 2*C*).

We next analysed the distribution of DGC components in DMD^{mdx} mice. As expected, we observed no labelling of intrafusal fibres with anti-dystrophin antibodies in DMD^{mdx} mice (Fig. 2*D*), demonstrating the specificity of the antibodies. Similar to extrafusal muscle fibres (Ibraghimov-Beskrovnaya *et al.* 1992; Rafael *et al.* 1994), the intensity of the β-dystroglycan immunoreactivity was considerably reduced in intrafusal fibres from DMD^{mdx} muscle spindles compared to wildtype muscle spindles (Fig. 2*E*). The weak residual immunoreactivity was distributed along the entire sarcolemma but the intensity was slightly higher in the contact region of intrafusal fibres with the sensory nerve ending (Fig. 2*E*′ and *E*′′), suggesting a redistribution of β-dystroglycan in DMD^{mdx} mice compared to wildtype mice. In contrast to the absence of anti-utrophin immunofluorescence signal in the central region of wildtype muscle spindles, we observed strong immunoreactivity for utrophin in the central region of intrafusal fibres from DMD^{mdx} mice (Fig. 2*F*). Moreover, the localization of utrophin immunofluorescence in muscle spindles from DMD^{mdx} mice recapitulated the differential labelling observed with anti-dystrophin antibodies in wildtype muscle spindles (Fig. 2*F*). Thus, utrophin appeared upregulated in the central region of intrafusal fibres of DMD^{mdx} mice. This suggests the possibility that utrophin compensates functionally and/or structurally for the absence of dystrophin.

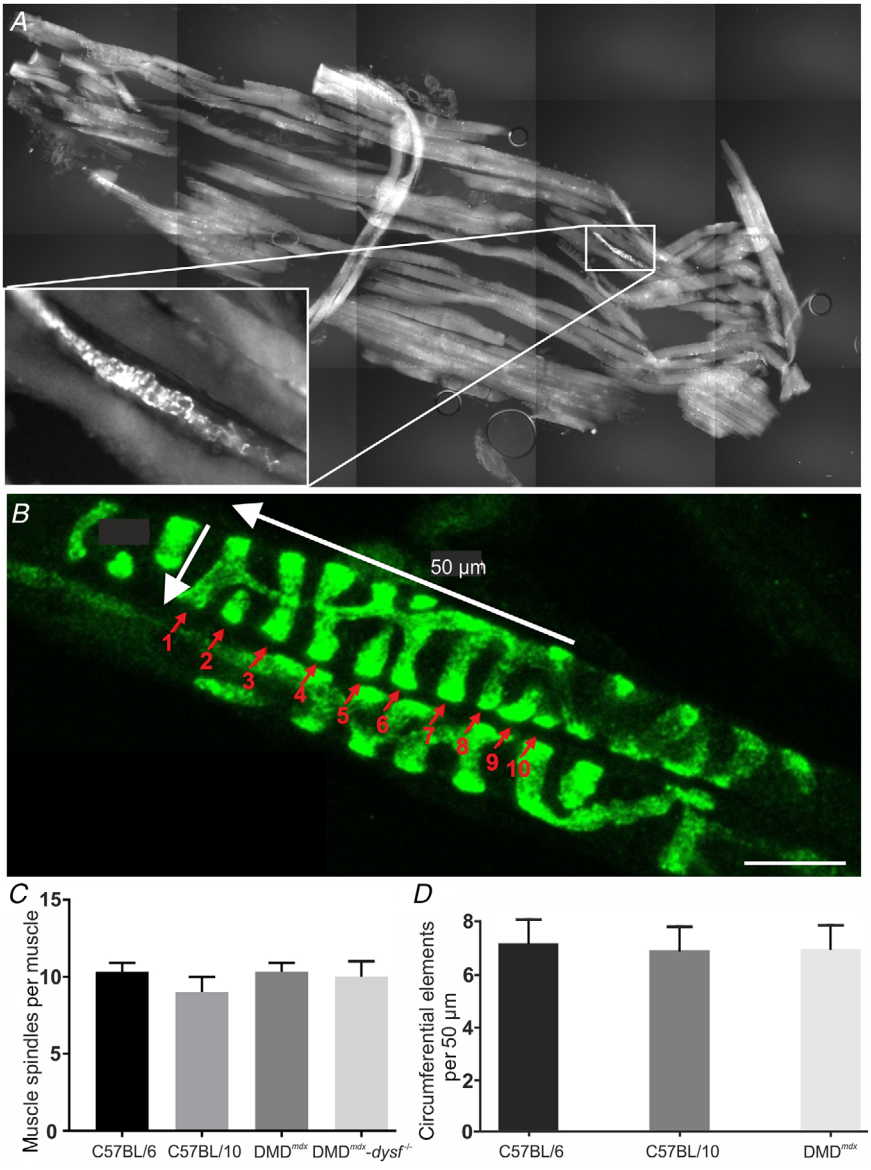

Figure 1. Structural analysis of muscle spindles from wildtype and dystrophic mice
The total number of muscle spindles was determined in soleus muscles by making tile scans of all sections of a soleus muscle. *A*, one individual tile scan of a wildtype C57BL/10 soleus muscle section stained with antibodies against vGluT1. An individual muscle spindle is shown at low and at high (inset) magnification. We observed no difference in the total number of muscle spindles in soleus muscles from wildtype or dystrophic mice (*C*). *B*, a muscle spindle from a DMD^{mdx} mouse stained with antibodies against vGluT1 to illustrate how the morphology of the sensory nerve terminal was analysed. The number of circumferential elements (indicated by red arrows and numbers in *B*) per 50 µm segment of intrafusal fibre was quantified in both wildtype and in DMD^{mdx} mice (*D*). There was no difference in the number of circumferential elements per 50 µm of intrafusal fibre length between wildtype and DMD^{mdx} mice. Scale bar in *B*: 10 µm [Colour figure can be viewed at wileyonlinelibrary.com]

To investigate the distribution of the DGC in a mouse model for MDs with an entirely different aetiology and molecular basis for the dystrophic phenotype, *dysf*$^{-/-}$ and DMD^{mdx}-*dysf*$^{-/-}$ double mutant mice were analysed and compared to *utrn*$^{-/-}$ and C57BL/10 wildtype mice. There was no apparent difference in the distribution of dystrophin between the two wildtype mouse strains (C57BL/6 and C57BL/10, respectively; compare Figs 2*A* and 3*A*). Likewise, we observed no difference in the localization of dystrophin and β-dystroglycan in muscle spindles from *utrn*$^{-/-}$ compared to C57BL/10 wildtype mice (Fig. 3*A*–*C*), suggesting that the distribution of the DGC in *utrn*$^{-/-}$ mice was similar to wildtype mice.

Dysferlin localizes to the plasma membrane and to the t-tubule system in wildtype extrafusal muscle fibres (Anderson *et al.* 1999; Ampong *et al.* 2005; Kerr *et al.* 2013). Accordingly, we observed a thin line of immunoreactivity with anti-dysferlin antibodies along the sarcolemma of extrafusal fibres (arrowheads in Fig. 3*F*). In addition, anti-dysferlin antibodies labelled parts of the sarcomeres, probably corresponding to the t-tubule system (Kerr *et al.* 2014). In the central region of intrafusal fibres, anti-dysferlin antibodies stained the plasma membrane (arrows in Fig. 3*F*). In addition, sarcomere-like structures similar to those stained in extrafusal fibres were observed in the polar contractile regions of intrafusal fibres (not shown). Dysferlin was also concentrated in the contact region between intrafusal fibres and the sensory nerve terminal (asterisks in Fig. 3*F*). No specific immunofluorescence signal was observed in muscle spindles from *dysf*$^{-/-}$ and in DMD^{mdx}-*dysf*$^{-/-}$ mice (Fig. 3*D* and *E*), demonstrating the specificity of the antibodies. Dystrophin was present and distributed similarly in wildtype and *dysf*$^{-/-}$ mice and was, as

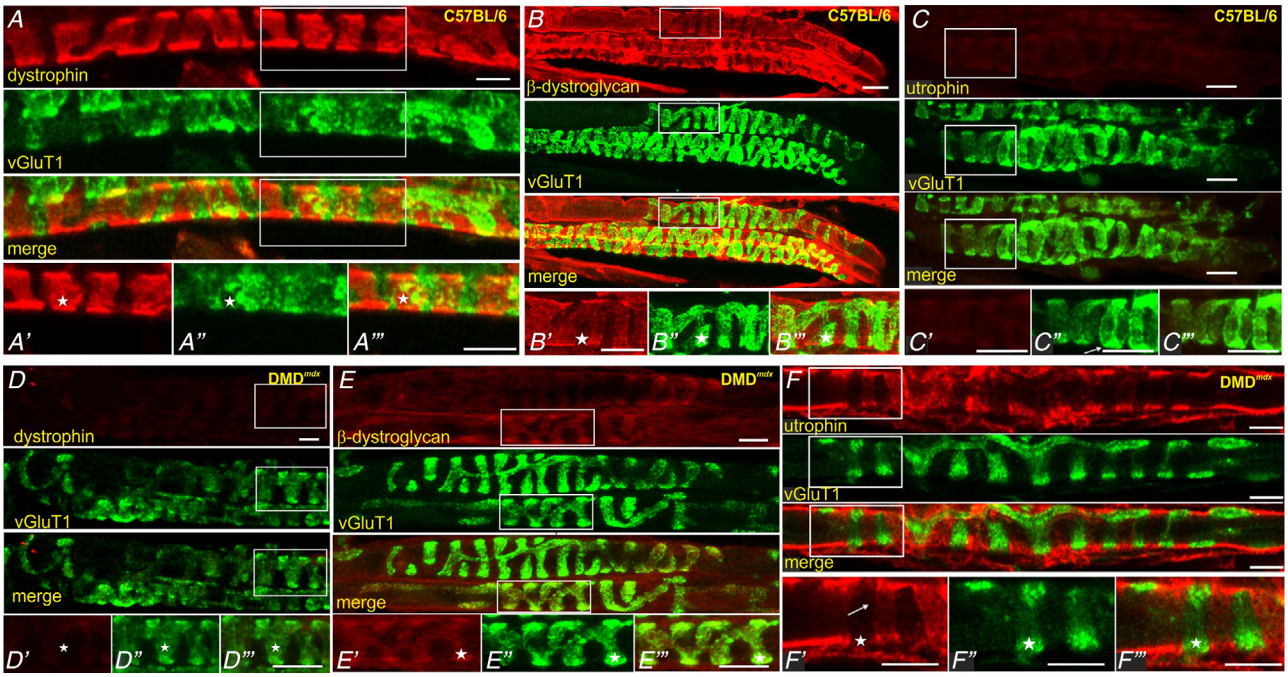

Figure 2. Distribution of DGC components in the equatorial region of muscle spindles from wildtype and DMD^{mdx} mice
The distribution of dystrophin (red channel in *A*, *D*), β-dystroglycan (red channel in *B*, *E*) and utrophin (red channel in *C*, *F*) was analysed in sections of soleus muscles from wildtype (*A*–*C*) and DMD^{mdx} (*D*–*F*) mice. Sections were stained with antibodies against vGluT1 (green channel in all panels) to illustrate the sensory nerve terminal. Insets at the bottom of each panel show the boxed areas at high magnification. Dystrophin (*A*′–*A*‴) and β-dystroglycan (*B*′–*B*‴) were present in intrafusal fibres but excluded from the region where the intrafusal fibre has direct contact to the sensory nerve terminal (marked by asterisks in *A*′–*A*‴ and *B*′–*B*‴). Utrophin was undetectable in the central region of wildtype intrafusal fibres (*C*). In contrast, the same antibodies strongly stained muscle spindles from DMD^{mdx} mice (*F*). In these mice, utrophin had the same subcellular distribution as dystrophin in wildtype muscle spindles (compare *A* and *F*). As expected, we observed no labelling with antibodies against dystrophin in DMD^{mdx} mice (*D*). The intensity of immunofluorescence staining with antibodies against β-dystroglycan appeared lower in DMD^{mdx} mice compared to wildtype mice (compare *B* and *E*) and labelling was observed along the entire sarcoplasm with a slightly higher intensity in the region of contact to the sensory neuron (*E*′–*E*‴). Asterisks mark corresponding areas in the insets. *E*, the same muscle spindle as in Fig. 1*B*. We observed a similar intensity and distribution of vGluT1 immunoreactivity in all mouse lines, suggesting an absence of major morphological changes in the sensory nerve terminal of the dystrophic mice. Scale bar in all panels: 10 μm. [Colour figure can be viewed at wileyonlinelibrary.com]

expected, absent in DMD^{mdx} and DMD^{mdx}-*dysf*$^{-/-}$ mice (Fig. 3*G* and *H*). We noted, however, a slight spreading of the immunoreactivity also into the area where the sensory neuron contacted the intrafusal muscle fibre (Fig. 3*G*). The distribution and intensity of the *β*-dystroglycan immunofluorescence were similar in wildtype and *dysf*$^{-/-}$ mice but were downregulated in DMD^{mdx}-*dysf*$^{-/-}$ mice similar to the reduced intensity of DMD^{mdx} mice (Fig. 3*I* and *J*). Thus, the subcellular localization of the DGC components in intrafusal fibres was very similar in wildtype and in *dysf*$^{-/-}$ mice, suggesting that any potential change in muscle spindle function in *dysf*$^{-/-}$ mice was unlikely to be due to a reduced expression or altered distribution of DGC proteins.

Muscle spindle afferents from DMD^{mdx} and *dysf*$^{-/-}$ mice have an increased resting discharge

To investigate if muscle spindle function is altered in DMD^{mdx} or *utrn*$^{-/-}$ mice, the discharge frequencies at four particular time points before and during ramp-and-hold stretches were recorded (Fig. 4) and compared to C57BL/10 wildtype control mice. We observed no difference in the resting discharge and in the response to ramp-and-hold stretches between C57BL/10 wildtype and *utrn*$^{-/-}$ mice (Fig. 5), suggesting that similar to extrafusal fibres, utrophin deficiency does not lead to functional deficits in muscle spindles. In DMD^{mdx} mice, the resting discharge frequency during the 10 s before the stretch

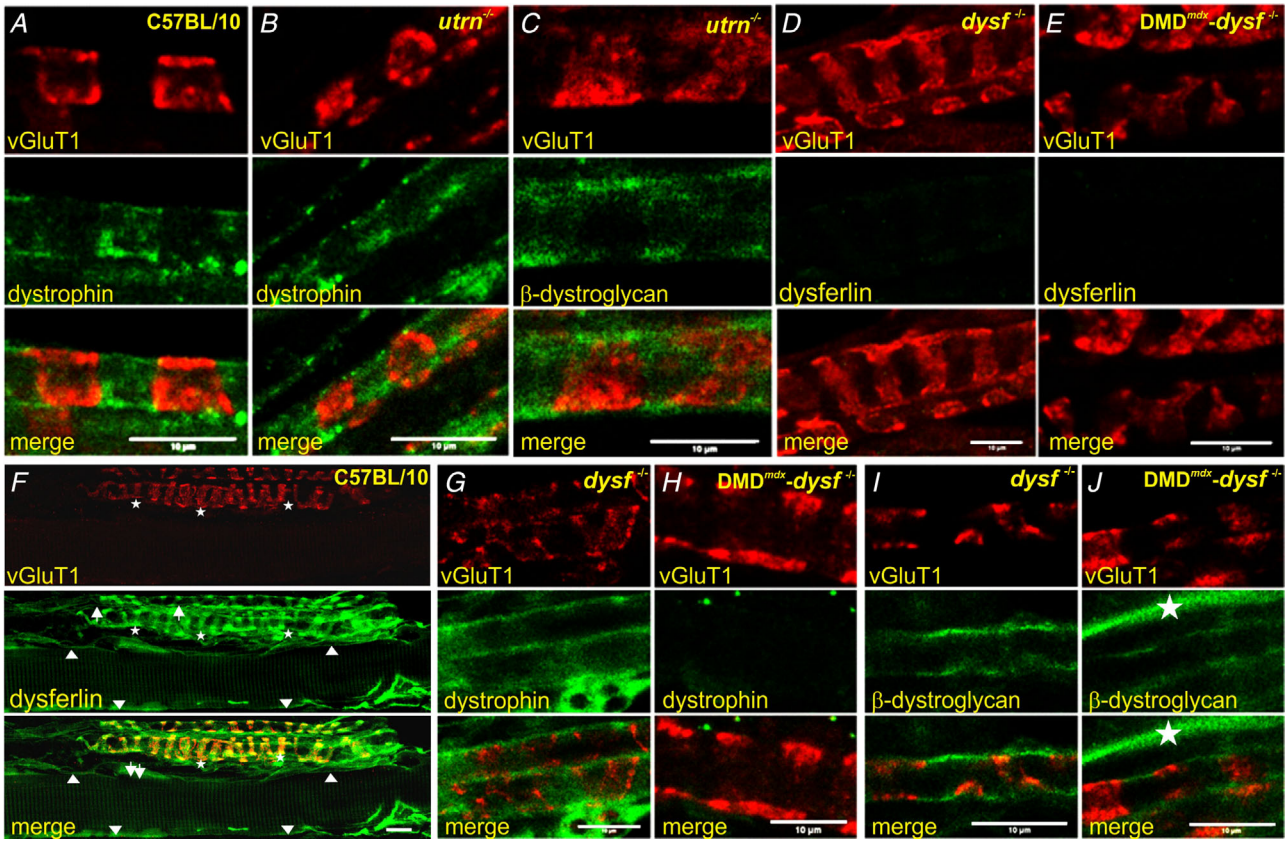

Figure 3. Distribution of dysferlin and DGC components in muscle spindles from wildtype and dystrophic mice
High-resolution confocal microscopy showing the subcellular distribution of dystrophin (green channel in *A*, *B*, *G*, *H*), *β*-dystroglycan (green channel in *C*, *I*, *J*) and dysferlin (green channel in *D*, *E*, *F*) in C57BL/10 wildtype (*A*, *F*), *utrn*$^{-/-}$ (*B*, *C*), *dysf*$^{-/-}$ (*D*, *E*, *G*, *I*) and DMD^{mdx}-*dysf*$^{-/-}$ (*H*, *J*) double mutant mice. The vGluT1 labelling (red channel in all panels) was used to label the sensory nerve terminal. Dystrophin had the same distribution in wildtype (*A*), *utrn*$^{-/-}$ (*B*) and *dysf*$^{-/-}$ (*G*) mice but was absent – as expected – from DMD^{mdx}-*dysf*$^{-/-}$ mice (*H*), i.e. dystrophin was subcellularly concentrated in the area of intrafusal fibres that did not have contact with the sensory nerve terminal. Dysferlin was present in the sarcolemmal plasma membrane and in parts of the sarcomere of extra- and intrafusal muscle fibres (arrowheads and arrows in *F*). The absence of immunoreactivity with antibodies against dysferlin in *dysf*$^{-/-}$ and of dysferlin and dystrophin in DMD^{mdx}-*dysf*$^{-/-}$ mice shows the specificity of the respective antibodies. *β*-Dystroglycan had the same distribution as dystrophin in *utrn*$^{-/-}$ (*C*), *dysf*$^{-/-}$ (*I*) and DMD^{mdx}-*dysf*$^{-/-}$ (*J*) mice. The asterisks in *J* mark the outer connective tissue capsule of the muscle spindle Scale bar in all panels: 10 µm. [Colour figure can be viewed at wileyonlinelibrary.com]

was significantly increased (Figs 4 and 5*A*). In contrast, the dynamic peak (Fig. 5*C*), dynamic index (Fig. 5*E*) and the static response (Fig. 5*G*) were not different in DMD^{mdx} muscle spindles compared to wildtype or *utrn*$^{-/-}$ mice. These results demonstrate an increased action potential frequency in DMD^{mdx} mice at rest and an apparently normal muscle spindle function in *utrn*$^{-/-}$ mice.

Small sinusoidal stretches can more specifically test the dynamic properties of muscle spindles (Brown *et al.* 1967; Hunt & Ottoson, 1977). We therefore investigated the response of muscle spindles from wildtype, *utrn*$^{-/-}$ and DMD^{mdx} mice to vibrational stimuli by exposing them to sinusoidal length changes of four different frequencies and four different amplitudes. Figure 6 shows a representative example of the responses of wildtype C57BL/6 (Fig. 6*A–C*) and DMD^{mdx} (Fig. 6*D–F*) muscle spindles to sinusoidal vibrations of 10 Hz frequency and 100 µm amplitude. The same stimulus induced more action potentials in dystrophic muscle compared to the wildtype control muscle. The passive mechanical tension generated at L_0 did not differ between wildtype and DMD^{mdx} mice (C57BL/6: 3.90 ± 0.22 mN, $N = 4$; DMD^{mdx}: 3.83 ± 0.23 mN, $N = 7$). Likewise, we did not observe obvious differences in the tension generated by the vibrations in wildtype (Fig. 6*B*) and DMD^{mdx} (Fig. 6*E*) mice, suggesting that the biomechanical properties of the EDL muscle were not apparently different in both mouse lines. The responses of muscle spindles to vibrational stimuli were expressed as impulses per 9 s (imp 9 s^{-1}; Wilkinson *et al.* 2012; Gerwin *et al.* 2019). Muscle spindles from DMD^{mdx} mice had a significantly higher number of action potentials per 9 s during low frequencies of 10 Hz at all four stretch amplitudes (triangles in Fig. 7*A–D*). However, with increasing frequencies, the muscle spindle responses in DMD^{mdx} mice became similar to the responses in wildtype (circles in Fig. 7*A–D*) and *utrn*$^{-/-}$ mice (squares in Fig. 7*A–D*). These results demonstrate an increased frequency of action potentials of muscle spindles from DMD^{mdx} mice in response to vibrations, particularly at low vibrational frequencies and small amplitudes, suggesting an increased dynamic sensitivity of muscle spindles in DMD^{mdx} mice.

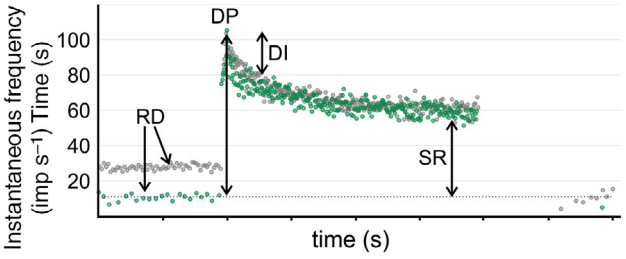

Figure 4. Resting discharge is increased in muscle spindles from DMD^{mdx} mice
Instantaneous frequency of muscle spindle responses to a ramp-and-hold stretch with a ramp speed of 40% L_0 s^{-1} and an overall 7.5% L_0 length change from a representative wildtype (green dots) and DMD^{mdx} (grey dots) mouse EDL muscle. The frequencies at four different time points before and during the stretch were subsequently quantified in wildtype and dystrophic mice (see Fig. 5): resting discharge (RD), dynamic peak (DP), dynamic index (DI) and static response (SR). While the resting discharge frequency was increased in DMD^{mdx} mice compared to C57BL/10 control mice, the other parameters were not apparently affected. The dotted line indicates the mean of the resting discharge of the wildtype muscle spindle. [Colour figure can be viewed at wileyonlinelibrary.com]

To investigate if muscle spindle function was similarly altered in an entirely different mouse model for MDs, *dysf*$^{-/-}$ and DMD^{mdx}-*dysf*$^{-/-}$ double mutant mice were analysed. Because these mice have a different genetic background, and because strain-dependent variations in muscle spindle structure have been reported (Lionikas *et al.* 2013), C57BL/6 mice were used as wildtype controls. Muscle spindle afferent discharge frequencies before and during ramp-and-hold stretches were recorded and analysed as described above. The resting discharge was significantly increased in both mutant lines compared to wildtype control mice (Fig. 5*B*). On the other hand, the parameters describing the dynamic phase (dynamic peak, Fig. 5*D*; dynamic index, Fig. 5*F*), as well as the static response to muscle stretch (Fig. 5*H*) were not altered in *dysf*$^{-/-}$ or DMD^{mdx}-*dysf*$^{-/-}$ mice compared to wildtype mice. These results indicate an increased action potential frequency in *dysf*$^{-/-}$ and DMD^{mdx}-*dysf*$^{-/-}$ mice at rest, which appeared similar to the increase observed in DMD^{mdx} mice. Moreover, we observed no additive effect in DMD^{mdx}-*dysf*$^{-/-}$ double mutant mice compared to either single mutant mouse line.

To study muscle spindle activity more specifically during the dynamic phase of a muscle stretch, muscle spindle afferent discharge responses to sinusoidal vibrations were analysed in *dysf*$^{-/-}$ and DMD^{mdx}-*dysf*$^{-/-}$ mice. Muscle spindles from *dysf*$^{-/-}$ (squares in Fig. 7*E–H*) and DMD^{mdx}-*dysf*$^{-/-}$ mice (triangles in Fig. 7*E–H*) had a significantly higher number of impulses per 9 s during small-amplitude vibrations (5 µm) at all frequencies (Fig. 7*E*). In contrast, the response to vibrations with larger amplitudes and higher frequencies were mostly similar to control values (Fig. 7*F–H*). We observed no difference in the response to sinusoidal vibrations between *dysf*$^{-/-}$ and DMD^{mdx}-*dysf*$^{-/-}$ mice (Fig. 7*E–H*), again demonstrating that there is no apparent additive effect of the two mutations. These results confirm an increased dynamic sensitivity of muscle spindles from dystrophic mice in their response to small-amplitude vibrations. In conclusion, our results demonstrate a qualitatively and quantitatively comparable increase in the resting discharge and in the response to vibrations in DMD^{mdx} and *dysf*$^{-/-}$ mice and no additive effect in the double mutant mice.

Discussion

Muscle spindles are sensors for proprioceptive stimuli and an impaired muscle spindle function contributes to several neuromuscular and neurodegenerative diseases (for reviews see Blecher *et al.* 2018; Kröger, 2018). We show that muscle spindle afferents from two dystrophic mouse lines with mutations in different genes and with different molecular mechanisms causing the muscle degeneration have a qualitatively and quantitatively similar increase in the resting discharge frequency and in the response to sinusoidal vibrations. We also show that the overall structure, total number of muscle spindles and their

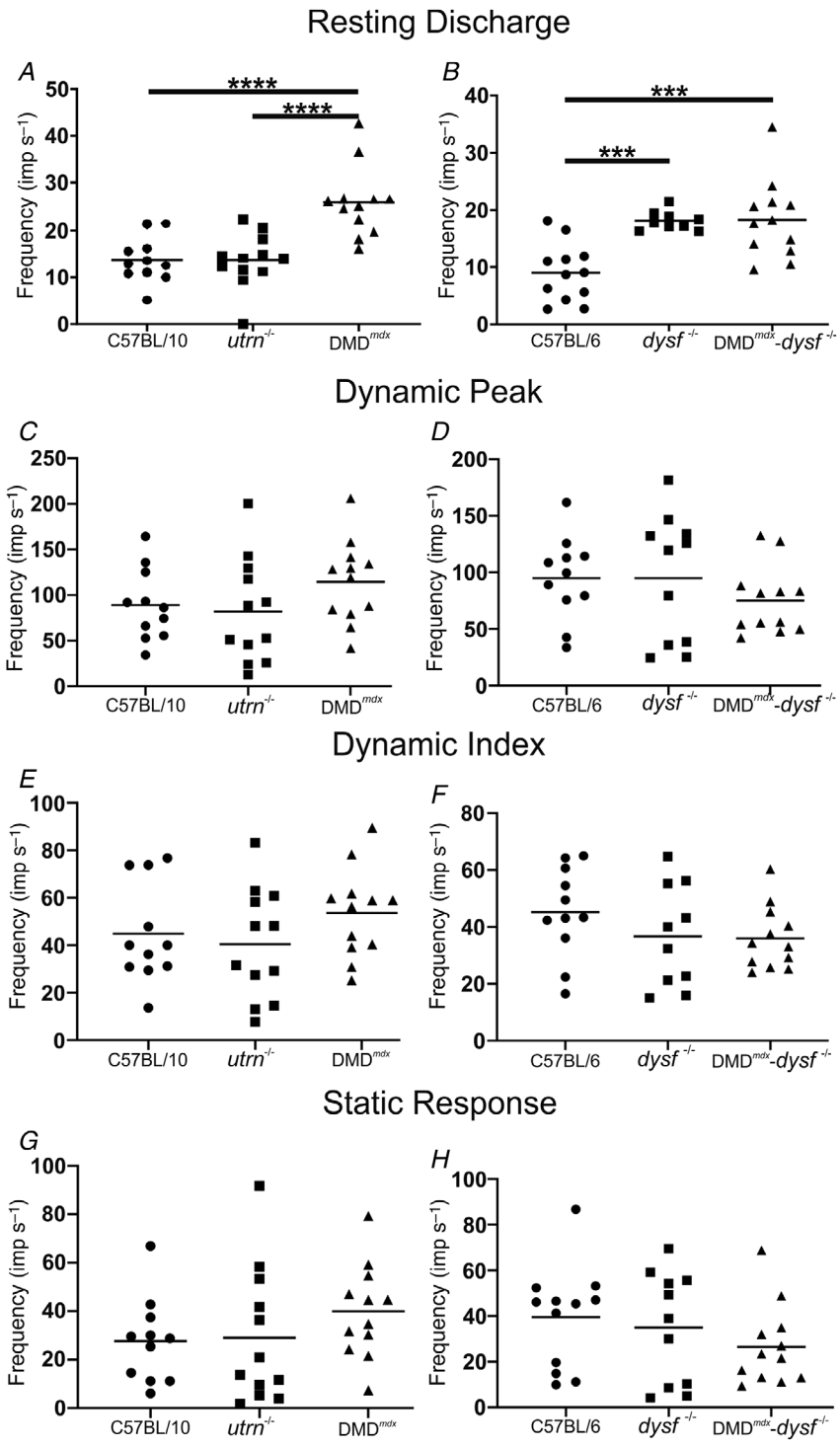

Figure 5. Resting discharge of muscle spindle afferents from DMD^{mdx}, *dysf* $^{-/-}$ and DMD^{mdx}-*dysf* $^{-/-}$ mice is increased but the muscle spindle response to ramp-and-hold stretches is unaltered
Discharge frequencies at rest (*A*, *B*), dynamic peak (*C*, *D*), dynamic index (*E*, *F*) and static response (*G*, *H*) were determined and compared between muscle spindles from wildtype (circles in *A*–*H*) and dystrophic mice. While the resting discharge was increased in the dystrophic mice, it was unaltered in wildtype and *utrn*$^{-/-}$ mice. We observed no additive effect of the resting discharge frequency change in the DMD^{mdx}-*dysf* $^{-/-}$ double mutant mice. The horizontal bar indicates the mean of the different experiments. Only significant differences are indicated. Each dot represents an independent experiment. Statistical significance of differences in the frequencies was determined using one-way ANOVA with Dunnett's multiple comparison test.

responses to ramp-and-hold stretches were not affected by the mutations. These results demonstrate that intrafusal fibres from dystrophic mice are less affected by the degenerative events compared to extrafusal fibres, but muscle spindles are nevertheless functionally impaired.

In a previous study, the localization of dystrophin in the central part of intrafusal fibres, with dystrophin-deficient segments alternating with positively stained domains along the sarcolemma, has been reported (Nahirney & Ovalle, 1993). We confirmed this finding using a different anti-dystrophin antibody and additionally show that other components of the DGC (i.e. β-dystroglycan) are similarly subcellularly concentrated in the same segments of the sarcoplasmic membrane. These segments coextend with the parts of intrafusal fibres that are in direct contact with the basal lamina (Maier & Mayne, 1995). In contrast, the intrafusal fibre plasma membrane is separated from the basal lamina by the sensory nerve terminal in the DGC-deficient segments. Thus, it is tempting to speculate that the DGC in intrafusal fibres is stabilized in the regions between the sensory nerve terminals by the direct contact to the extracellular matrix. The absence of dystrophin and β-dystroglycan immunoreactivity in the contact region between the sensory neuron and the intrafusal fibre also suggests that the DGC is not directly involved in the mechanotransduction process. It remains to be shown if the DGC is actively excluded from the sensory neuron to intrafusal fibre contact zone or if it is not stabilized in regions where intrafusal fibres have no contact to the basal lamina.

Analysis of muscle tissue from MD patients has revealed conflicting results regarding changes in the overall morphology of muscle spindles. Some studies have reported that muscle spindle morphology in post-mortem muscle tissue was slightly atrophic and that due to the loss of intrafusal fibres and a reduced intrafusal fibre diameter, the periaxial space was increased and the connective tissue capsule was widened (Swash & Fox, 1976; Kararizou *et al.* 2007). In contrast, other studies analysing intrafusal fibres in biopsy material from

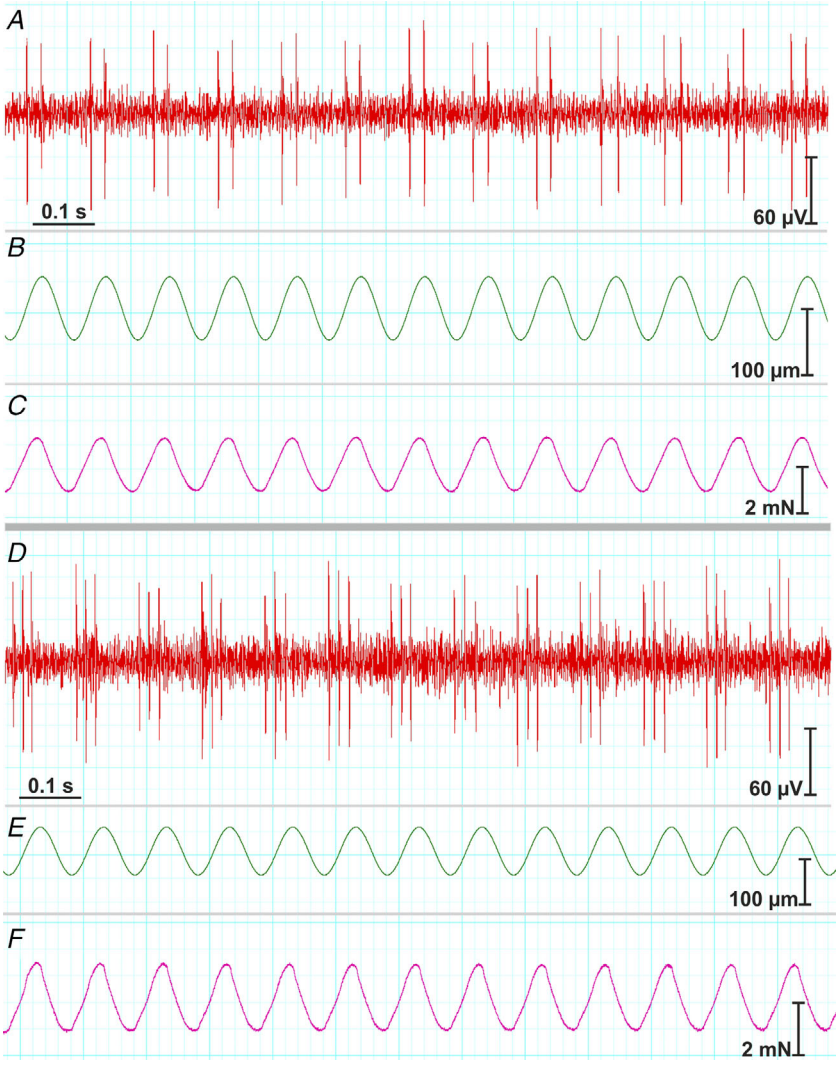

Figure 6. Increased firing frequency of muscle spindle sensory afferents from DMD^{mdx} mice in response to sinusoidal vibrations
The response of a single representative muscle spindle afferent from wildtype (*A*) and DMD^{mdx} (*D*) mice to sinusoidal vibrations of 10 Hz and 100 µm amplitude. Corresponding length changes (stretch is represented as an upward deflection) and the passive mechanical tension, generated by the muscle in response to the vibration, are shown in *B* and *C*, respectively, for wildtype and in *E* and *F* for DMD^{mdx} mice. Note that more action potentials are generated in DMD^{mdx} mice compared to wildtype control mice. The tension generated by the muscle in response to the stimuli is similar in wildtype (*C*) and DMD^{mdx} muscle (*F*). [Colour figure can be viewed at wileyonlinelibrary.com]

patients showed a normal diameter and an unaltered thickness of the connective tissue capsule (Cazzato & Walton, 1968; Skuk *et al.* 2010). It is therefore possible that the morphological changes observed in the first two studies were not a direct consequence of the mutation but instead caused by secondary effects, including age, immobilization or post-mortem tissue autolysis. Regardless, compared to extrafusal fibres, intrafusal fibres and muscle spindle structure appear much less affected by the mutation. This is consistent with our finding that in the DMD^{mdx} mouse, the morphological changes appeared to be considerably less pronounced compared to those described for extrafusal fibres.

We observed no apparent degeneration of intrafusal fibres or a reduction in the total number of muscle spindles per soleus muscle. Likewise, the distribution of the vGluT1 immunoreactivity was not apparently different in the central region of intrafusal fibres in muscle spindles from the various dystrophic mice. One potential explanation for the mild phenotypic effect of the mutations might be that intrafusal fibres have a much smaller mechanical burden and are thus less likely to suffer from mechanical damage. An additional possibility is suggested by our finding that utrophin expression was markedly upregulated in the DMD^{mdx} mouse. Utrophin is an autosomally encoded paralogue of dystrophin, which shares more than 80% amino acid sequence similarity to dystrophin, has a very similar domain structure, and like dystrophin can interact with actin filaments and with β-dystroglycan (Tinsley *et al.* 1992). In skeletal muscle, utrophin is highly expressed in fetal and regenerating muscle fibres (Khurana *et al.* 1991; Lin *et al.* 1998). In adult wildtype muscle fibres, utrophin is replaced by dystrophin along the entire sarcolemmal membrane but remains present at the neuromuscular

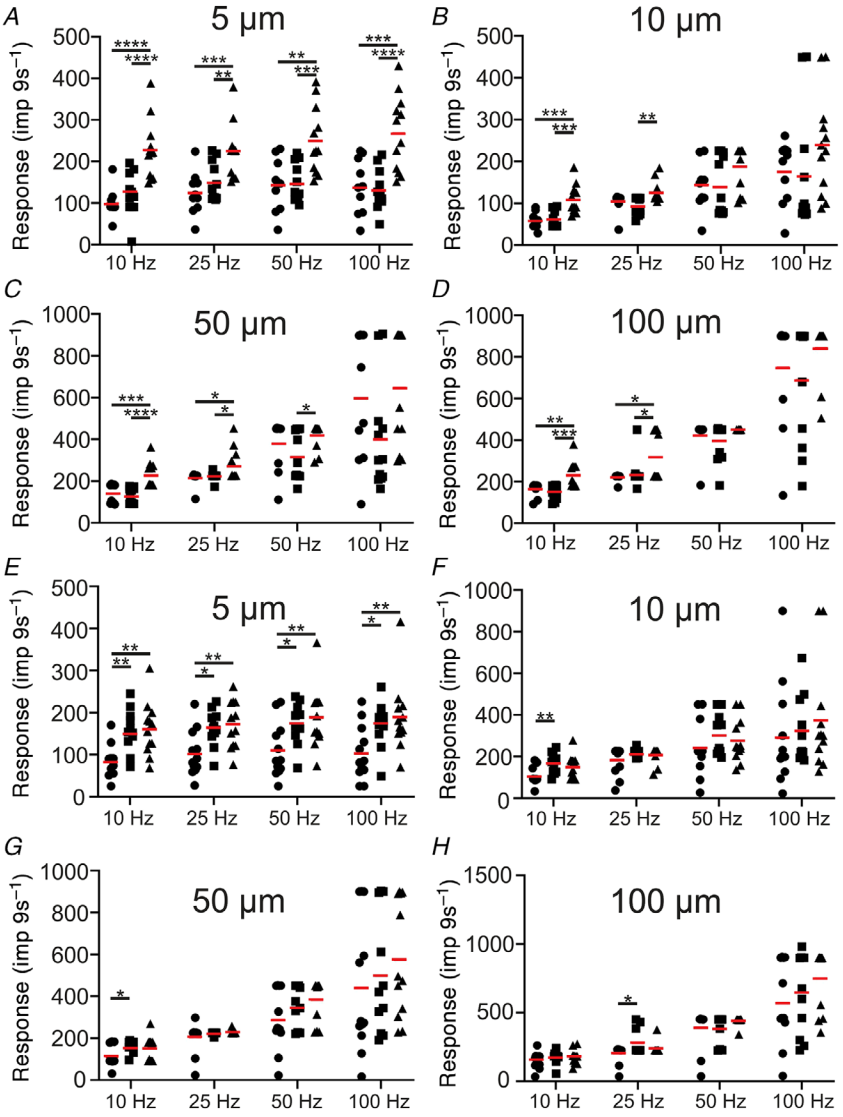

Figure 7. Responses of muscle spindles from wildtype and dystrophic mice to sinusoidal vibrations
A–D, muscle spindle afferent responses (imp 9 s^{-1}) to vibrational stimuli with frequencies of 10, 25, 50 and 100 Hz and amplitudes of 5, 10, 50 and 100 µm determined in C57BL/10 (circles), *utrn*$^{-/-}$ (squares) and DMD^{mdx} (triangles) mice. Responses to vibrational stimuli of 10 and 25 Hz were different in wildtype compared to DMD^{mdx} mice at all amplitudes, but the differences declined at higher frequencies and amplitudes. In contrast, responses of muscle spindles from *utrn*$^{-/-}$ mice were similar to wildtype spindles at all amplitudes and frequencies. *E–H*, responses of muscle spindles from C57BL/6 (circles), *dysf* $^{-/-}$ (squares) and DMD^{mdx}-*dysf* $^{-/-}$ (triangles) mice to the same vibrational stimuli as in *A–D*. The frequencies were increased in both mutant mouse lines particularly at small amplitudes and low frequencies. No significant differences were found at higher amplitudes and frequencies. We observed no additive effect in the DMD^{mdx}-*dysf*$^{-/-}$ double mutant mice compared to both single mutant mice. Only significant differences are indicated. The red bar represents the mean of the frequencies. Statistical significance was determined using one-way ANOVA with Dunnett's multiple comparison test. [Colour figure can be viewed at wileyonlinelibrary.com]

junction, the myo-tendinous junction and blood vessels (Nguyen *et al.* 1991; Ohlendieck *et al.* 1991; Bewick *et al.* 1992; Schofield *et al.* 1993). In DMD^{mdx} mice, utrophin is greatly upregulated in extrafusal fibres and can be found along the entire sarcolemma (Pons *et al.* 1993; Hirst *et al.* 2005). Upregulation of utrophin expression can lessen or even prevent the dystrophic phenotype in DMD^{mdx} mice and MD patients (Tinsley *et al.* 1998, 2011; Gilbert *et al.* 1999; Hirst *et al.* 2005; Amenta *et al.* 2011; Davies & Chamberlain, 2019; Guiraud *et al.* 2019). We therefore suggest that a similar functional compensation occurs endogenously in intrafusal fibres, resulting in a less severe phenotype in DMD^{mdx} mice. In contrast, in human DMD patients utrophin is only slightly increased at the sarcolemma of regenerating extrafusal fibres during the repair process (Helliwell *et al.* 1992; Guiraud *et al.* 2019). Likewise, intrafusal fibres in DMD patients do not apparently upregulate utrophin expression (Skuk *et al.* 2010), predicting more severe functional deficits in human muscle spindles compared to those from DMD^{mdx} mice.

The *dysf*$^{-/-}$ mice used in this study have a 171 bp deletion (Vafiadaki *et al.* 2001) and a reduction of functional dysferlin to ∼15% of the value for normal skeletal muscle fibres (Bittner *et al.* 1999). This reduced dysferlin expression leads to an impairment of the sarcolemmal membrane repair machinery and subsequently to a degeneration of extrafusal muscle fibres (Bansal *et al.* 2003; Cardenas *et al.* 2016; Barthelemy *et al.* 2018). In contrast, mutations in dystrophin affect the mechanical stability of muscle fibres, rendering them mechanically labile, so that the sarcolemmal membrane has a higher susceptibility to damage, particularly during contraction (Waite *et al.* 2012). Extrafusal muscle fibres are much less affected in *dysf*$^{-/-}$ mice compared to the DMD^{mdx} mice and only a minority of fibres have centrally localized nuclei (Nemoto *et al.* 2007). Likewise, no change in the distribution of DGC components was reported in extrafusal fibres from *dysf*$^{-/-}$ mice (Matsuda *et al.* 1999; Bansal *et al.* 2003). Similarly, muscle weakness is mild in young *dysf*$^{-/-}$ mice compared to animals older than 8 months (Hornsey *et al.* 2013; Terrill *et al.* 2013). Despite these extensive differences between *dysf*$^{-/-}$ and DMD^{mdx} mice, muscle spindle afferents from both mouse strains were strikingly similarly affected. Both showed an increase in the resting discharge and an altered response to sinusoidal vibrations particularly at small amplitudes but no change in the response to ramp-and-hold stretches. Moreover, there was no additive effect in double mutant mice and no change in the distribution of dystrophin in *dysf*$^{-/-}$ mice, suggesting that both mutations phenotypically converge onto a common intracellular signalling pathway.

The molecular mechanism underlying the increase in the resting discharge in dystrophic muscles is unclear. After shortening in our assay system, muscle spindles fall silent but the original resting discharge frequency is gradually reached again after several seconds. In cat soleus muscle, an early recovery could be induced by specifically stimulating static- but not dynamic γ-motoneurons, suggesting that the resting discharge frequency in cat muscle spindles is primarily mediated by bag_2 fibres (Proske *et al.* 1991). Thus, a selective effect of the mutations on bag_2 fibres could be one way to explain the increased resting discharge. We did not observe a difference in the distribution of dystrophin, β-dystroglycan or utrophin in wildtype or dystrophic mice between nuclear bag and nuclear chain fibres. The mutations in these proteins are therefore unlikely to selectively affect bag_2 intrafusal fibres. Likewise, we cannot exclude an effect of the mutations on the viscoelastic properties specifically of bag_2 fibres, although the passive mechanical tension generated at L_0 length and during the vibrational stimuli appeared similar in wildtype and dystrophic mice.

An alternative explanation for the similar increase in the resting discharge of both dystrophic mice might be a change in the intracellular calcium ion concentration [Ca^{2+}]. Several studies have shown an abnormal calcium-ion homeostasis in extrafusal fibres in murine models of both MD types (Turner *et al.* 1988, 1993; Franco & Lansman, 1990; Mallouk *et al.* 2000; Robert *et al.* 2001; Vandebrouck *et al.* 2002; Klinge *et al.* 2010; Flix *et al.* 2013; Kerr *et al.* 2013). Dysferlin is localized in the t-tubule membrane and physically associated with the dihydropyridine receptor and several other proteins involved in Ca^{2+}-based signalling (Ampong *et al.* 2005; de Morree *et al.* 2010; Klinge *et al.* 2010; Waddell *et al.* 2011; Hornsey *et al.* 2013; Kerr *et al.* 2013). In addition, blocking of L-type Ca^{2+} channels in the t-tubule membrane using diltiazem improves the recovery of *dysf*$^{-/-}$ muscle fibres from injury (Kerr *et al.* 2013). Collectively, these results suggest that calcium ions might play a pivotal role in the aetiology of the dystrophic phenotype in extrafusal fibres from both mouse strains. In line with these findings, we hypothesize that an elevated cytosolic Ca^{2+} concentration under resting conditions as the mechanistic link between the genetic defect and the dystrophic phenotype in muscle spindles from both mouse models of MD. An increased Ca^{2+} concentration in intrafusal fibres would presumably lead to a contraction in the polar regions. This would exert stretch in the central equatorial region causing an elevated discharge frequency of the proprioceptive sensory ending. It will therefore be interesting to investigate if the intracellular Ca^{2+} concentration is elevated and if the Ca^{2+} homeostasis is perturbed in muscle spindles from both dystrophic mouse lines.

Postural abnormalities have been reported previously in patients with MD of the Duchenne type and in dysferlinopathies (Hsu & Furumasu, 1993; Mahjneh *et al.* 2001; Pradhan *et al.* 2006). In general, MD patients suffer

from sudden spontaneous falls, balance problems, as well as gait and posture abnormalities (Barrett *et al.* 1988) or kinematic and mechanical deficits as well as a peripheral areflexia (Fukuda *et al.* 1999; Umakhanova *et al.* 2017). Some of these symptoms can certainly be attributed to the muscle weakness. However, a disturbance in proprioception may also contribute to the impaired postural control in these patients. Analyses of the perception of body segment movement and control of posture in patients suffering from various types of MD failed to reveal differences between MD patients and healthy subjects (Ribot-Ciscar *et al.* 2004). Both MD patients and healthy subjects perceived passive movements and experienced sensations of illusory movement induced by vibratory stimulation applied to muscle tendons, suggesting that muscle spindles are still responsive to vibratory stimulation and that proprioception in general might be spared in MD patients or that the defects of muscle spindles are compensated for (Ribot-Ciscar *et al.* 2004). Moreover, the effects of reinforcement manoeuvres that are known to increase muscle spindle sensitivity via fusimotor drive in healthy subjects were unaltered in MD patents, suggesting that the intrafusal muscle fibres preserve their contractile abilities in slowly progressive MDs (Aimonetti *et al.* 2005). Our results showing that the dynamic and static responses to stretch were unaltered in DMD^{mdx} mice are in agreement with these studies. However, we observed an increase in the resting discharge of muscle spindle afferents and an altered response to sinusoidal vibrations. It is unclear how much these alterations affect proprioception, because muscle spindle afferent information is highly processed in the CNS (Proske & Gandevia, 2012; Proske & Gandevia, 2018). However, the increased resting discharge frequency could also directly feed back on skeletal muscle tissue via the monosynaptic stretch reflex. Accordingly, an increased resting discharge of sensory afferents might lead to an increase in muscle tone in the patients. This could not only cause postural problems but also increase the stiffness and by this enhance the degeneration of extrafusal fibres in dystrophic patients.

References

Aimonetti JM, Ribot-Ciscar E, Rossi-Durand C, Attarian S, Pouget J & Roll JP (2005). Functional sparing of intrafusal muscle fibers in muscular dystrophies. *Muscle Nerve* **32**, 88–94.

Amenta AR, Yilmaz A, Bogdanovich S, McKechnie BA, Abedi M, Khurana TS & Fallon JR (2011). Biglycan recruits utrophin to the sarcolemma and counters dystrophic pathology in mdx mice. *Proc Natl Acad Sci U S A* **108**, 762–767.

Ampong BN, Imamura M, Matsumiya T, Yoshida M & Takeda S (2005). Intracellular localization of dysferlin and its association with the dihydropyridine receptor. *Acta Myol* **24**, 134–144.

Anderson LV, Davison K, Moss JA, Young C, Cullen MJ, Walsh J, Johnson MA, Bashir R, Britton S, Keers S, Argov Z, Mahjneh I, Fougerousse F, Beckmann JS & Bushby KM (1999). Dysferlin is a plasma membrane protein and is expressed early in human development. *Hum Mol Genet* **8**, 855–861.

Aoki M, Liu J, Richard I, Bashir R, Britton S, Keers SM, Oeltjen J, Brown HE, Marchand S, Bourg N, Beley C, McKenna-Yasek D, Arahata K, Bohlega S, Cupler E, Illa I, Majneh I, Barohn RJ, Urtizberea JA, Fardeau M, Amato A, Angelini C, Bushby K, Beckmann JS & Brown RH, Jr (2001). Genomic organization of the dysferlin gene and novel mutations in Miyoshi myopathy. *Neurology* **57**, 271–278.

Banks RW (1994). The motor innervation of mammalian muscle-spindles. *Prog Neurobiol* **43**, 323–362.

Banks RW (2015). The innervation of the muscle spindle: a personal history. *J Anat* **227**, 115–135.

Bansal D, Miyake K, Vogel SS, Groh S, Chen CC, Williamson R, Mcneil PL & Campbell KP (2003). Defective membrane repair in dysferlin-deficient muscular dystrophy. *Nature* **423**, 168–172.

Barrett R, Hyde SA, Scott OM & Dubowitz V (1988). Changes in center of gravity in boys with Duchenne muscular dystrophy. *Muscle Nerve* **11**, 1157–1163.

Barthelemy F, Defour A, Levy N, Krahn M & Bartoli M (2018). Muscle cells fix breaches by orchestrating a membrane repair ballet. *J Neuromuscul Dis* **5**, 21–28.

Barton ER, Wang BJ, Brisson BK & Sweeney HL (2010). Diaphragm displays early and progressive functional deficits in dysferlin-deficient mice. *Muscle Nerve* **42**, 22–29.

Bashir R, Britton S, Strachan T, Keers S, Vafiadaki E, Lako M, Richard I, Marchand S, Bourg N, Argov Z, Sadeh M, Mahjneh I, Marconi G, Passos-Bueno MR, Moreira Ede S, Zatz M, Beckmann JS & Bushby K (1998). A gene related to Caenorhabditis elegans spermatogenesis factor fer-1 is mutated in limb-girdle muscular dystrophy type 2B. *Nat Genet* **20**, 37–42.

Bewick GS & Banks RW (2015). Mechanotransduction in the muscle spindle. *Pflugers Archiv: Eur J Physiol* **467**, 175–190.

Bewick GS, Nicholson LVB, Young C, O'Donnell E & Slater CR (1992). Different distributions of dystrophin and related proteins at nerve-muscle junctions. *Neuroreport* **3**, 857–860.

Bittner RE, Anderson LVB, Burkhardt E, Bashir R, Vafiadaki E, Ivanova S, Raffelsberger T, Maerk I, Hoger H, Jung M, Karbasiyan M, Storch M, Lassmann H, Moss JA, Davison K, Harrison R, Bushby KMD & Reis A (1999). Dysferlin deletion in SJL mice (SJL-Dysf) defines a natural model for limb girdle muscular dystrophy 2B. *Nat Genet* **23**, 141–142.

Blake DJ & Kröger S (2000). The neurobiology of Duchenne muscular dystrophy: learning lessons from muscle? *Trends Neurosci* **23**, 92–99.

Blecher R, Heinemann-Yerushalmi L, Assaraf E, Konstantin N, Chapman JR, Cope TC, Bewick GS, Banks RW & Zelzer E (2018). New functions for the proprioceptive system in skeletal biology. *Phil Trans Royal Soc Series B, Biol Sci* **373**, 20170327.

Brooks SV & Faulkner JA (1988). Contractile properties of skeletal muscles from young, adult and aged mice. *J Physiol* **404**, 71–82.

Brown MC, Engberg I & Matthews PB (1967). The use of vibration as a selective repetitive stimulus for Ia afferent fibres. *J Physiol* **191**, 31P-32P.

Bulfield G, Siller WG, Wight PA & Moore KJ (1984). X chromosome-linked muscular dystrophy (mdx) in the mouse. *Proc Natl Acad Sci USA* **81**, 1189–1192.

Campbell KP & Kahl SD (1989). Association of dystrophin and an integral membrane glycoprotein. *Nature* **338**, 259–262.

Cardenas AM, Gonzalez-Jamett AM, Cea LA, Bevilacqua JA & Caviedes P (2016). Dysferlin function in skeletal muscle: Possible pathological mechanisms and therapeutical targets in dysferlinopathies. *Exp Neurol* **283**, 246–254.

Cazzato G & Walton JN (1968). The pathology of the muscle spindle. A study of biopsy material in various muscular and neuromuscular diseases. *J Neurol Sci* **7**, 15–70.

Chang NC, Chevalier FP & Rudnicki MA (2016). Satellite cells in muscular dystrophy - lost in polarity. *Trends Mol Med* **22**, 479–496.

Constantin B (2014). Dystrophin complex functions as a scaffold for signalling proteins. *Biochim Biophys Acta* **1838**, 635–642.

Davies KE & Chamberlain JS (2019). Surrogate gene therapy for muscular dystrophy. *Nat Med* **25**, 1470–1476.

De-Doncker L, Picquet F, Petit J & Falempin M (2003). Effects of hypodynamia-hypokinesia on the muscle spindle discharges of rat soleus muscle. *J Neurophysiol* **89**, 3000–3007.

de Morree A, Hensbergen PJ, van Haagen HH, Dragan I, Deelder AM, t Hoen PA, Frants RR & van der Maarel SM (2010). Proteomic analysis of the dysferlin protein complex unveils its importance for sarcolemmal maintenance and integrity. *PLoS One* **5**, e13854.

Deconinck AE, Potter AC, Tinsley JM, Wood SJ, Vater R, Young C, Metzinger L, Vincent A, Slater CR & Davies KE (1997). Postsynaptic abnormalities at the neuromuscular junctions of utrophin-deficient mice. *J Cell Biol* **136**, 883–894.

Dietz V (2002). Proprioception and locomotor disorders. *Nature Rev Neurosci* **3**, 781–790.

Dillingham BC, Benny Klimek ME, Gernapudi R, Rayavarapu S, Gallardo E, Van der Meulen JH, Jordan S, Ampong B, Gordish-Dressman H, Spurney CF & Nagaraju K (2015). Inhibition of inflammation with celastrol fails to improve muscle function in dysferlin-deficient A/J mice. *J Neurol Sci* **356**, 157–162.

Ervasti JM (2007). Dystrophin, its interactions with other proteins, and implications for muscular dystrophy. *Biochim Biophys Acta* **1772**, 108–117.

Flix B, de la Torre C, Castillo J, Casal C, Illa I & Gallardo E (2013). Dysferlin interacts with calsequestrin-1, myomesin-2 and dynein in human skeletal muscle. *Int J Biochem Cell Biol* **45**, 1927–1938.

Franco A, Jr. & Lansman JB (1990). Calcium entry through stretch-inactivated ion channels in *mdx* myotubes. *Nature* **344**, 670–673.

Franco JA, Kloefkorn HE, Hochman S & Wilkinson KA (2014). An *in vitro* adult mouse muscle-nerve preparation for studying the firing properties of muscle afferents. *J Vis Exp*, 51948.

Fukuda K, Koto A, Fukuuchi Y & Ishihara T (1999). Characteristic form of standing up from squatting in Miyoshi's distal muscular dystrophy. *Clin Neurol Neurosurg* **101**, 249–252.

Gao QQ & McNally EM (2015). The dystrophin complex: structure, function, and implications for therapy. *Compr Physiol* **5**, 1223–1239.

Gerwin L, Haupt C, Wilkinson KA & Kröger S (2019). Acetylcholine receptors in the equatorial region of intrafusal muscle fibres modulate mouse muscle spindle sensitivity. *J Physiol* **597**, 1993–2006.

Gilbert R, Nalbantoglu J, Petrof BJ, Ebihara S, Guibinga GH, Tinsley JM, Kamen A, Massie B, Davies KE & Karpati G (1999). Adenovirus-mediated utrophin gene transfer mitigates the dystrophic phenotype of mdx mouse muscles. *Hum Gene Ther* **10**, 1299–1310.

Goldstein JA & McNally EM (2010). Mechanisms of muscle weakness in muscular dystrophy. *J Gen Physiol* **136**, 29–34.

Grady RM, Merlie JP & Sanes JR (1997). Subtle neuromuscular defects in utrophin-deficient mice. *J Cell Biol* **136**, 871–882.

Guiraud S, Edwards B, Babbs A, Squire SE, Berg A, Moir L, Wood MJ & Davies KE (2019). The potential of utrophin and dystrophin combination therapies for Duchenne muscular dystrophy. *Hum Mol Genet* **28**, 2189–2200

Hakim CH, Grange RW & Duan D (2011). The passive mechanical properties of the extensor digitorum longus muscle are compromised in 2- to 20-mo-old mdx mice. *J Appl Physiol* **110**, 1656–1663.

Han R & Campbell KP (2007). Dysferlin and muscle membrane repair. *Curr Opin Cell Biol* **19**, 409–416.

Han R, Frett EM, Levy JR, Rader EP, Lueck JD, Bansal D, Moore SA, Ng R, Beltran-Valero de Bernabe D, Faulkner JA & Campbell KP (2010). Genetic ablation of complement C3 attenuates muscle pathology in dysferlin-deficient mice. *J Clin Invest* **120**, 4366–4374.

Han R, Rader EP, Levy JR, Bansal D & Campbell KP (2011). Dystrophin deficiency exacerbates skeletal muscle pathology in dysferlin-null mice. *Skeletal Muscle* **1**, 1–35.

Helliwell TR, Man NT, Morris GE & Davies KE (1992). The dystrophin-related protein, utrophin, is expressed on the sarcolemma of regenerating human skeletal muscle fibres in dystrophies and inflammatory myopathies. *Neuromuscul Disord* **2**, 177–184.

Hirst RC, McCullagh KJ & Davies KE (2005). Utrophin upregulation in Duchenne muscular dystrophy. *Acta Myol* **24**, 209–216.

Hornsey MA, Laval SH, Barresi R, Lochmüller H & Bushby K (2013). Muscular dystrophy in dysferlin-deficient mouse models. *Neuromuscular Disord* **23**, 377–387.

Horowits R, Dalakas MC & Podolsky RJ (1990). Single skinned muscle fibers in Duchenne muscular dystrophy generate normal force. *Ann Neurol* **27**, 636–641.

Hsu JD & Furumasu J (1993). Gait and posture changes in the Duchenne muscular dystrophy child. *Clin Orthopaed Rel Res* **288**, 122–125.

Hunt CC & Ottoson D (1977). Responses of primary and secondary endings of isolated mammalian muscle spindles to sinusoidal length changes. *J Neurophysiol* **40**, 1113–1120.

Ibraghimov-Beskrovnaya O, Ervasti JM, Leveille CJ, Slaughter CA, Sernett SW & Campbell KP (1992). Primary structure of dystrophin-associated glycoproteins linking dystrophin to the extracellular matrix. *Nature* **355**, 696–702.

Johnson MI & Ovalle WK. (1986). A comparative study of muscle spindles in slow and fast neonatal muscles of normal and dystrophic mice. *Am J Anat* **175**, 413–427.

Kararizou EG, Manta P, Kalfakis N, Gkiatas KA & Vassilopoulos D (2007). Morphologic and morphometrical study of the muscle spindle in muscular dystrophy. *Analyt Quantitat Cytol Histol* **29**, 148–152.

Kashkoush AI, Gaunt RA, Fisher LE, Bruns TM & Weber DJ (2019). Recording single- and multi-unit neuronal action potentials from the surface of the dorsal root ganglion. *Sci Rep* **9**, 2786.

Kerr JP, Ward CW & Bloch RJ (2014). Dysferlin at transverse tubules regulates Ca(2+) homeostasis in skeletal muscle. *Front Physiol* **5**, 89.

Kerr JP, Ziman AP, Mueller AL, Muriel JM, Kleinhans-Welte E, Gumerson JD, Vogel SS, Ward CW, Roche JA & Bloch RJ (2013). Dysferlin stabilizes stress-induced Ca^{2+} signaling in the transverse tubule membrane. *Proc Natl Acad Sci U S A* **110**, 20831–20836.

Khurana TS, Watkins SC, Chafey P, Chelly J, Tome FM, Fardeau M, Kaplan JC & Kunkel LM (1991). Immunolocalization and developmental expression of dystrophin related protein in skeletal muscle. *Neuromuscul Disord* **1**, 185–194.

Klinge L, Harris J, Sewry C, Charlton R, Anderson L, Laval S, Chiu YH, Hornsey M, Straub V, Barresi R, Lochmüller H & Bushby K (2010). Dysferlin associates with the developing T-tubule system in rodent and human skeletal muscle. *Muscle Nerve* **41**, 166–173.

Kröger S (2018). Proprioception 2.0: novel functions for muscle spindles. *Curr Opin Neurol* **31**, 592–598.

Larsson L & Edstrom L (1986). Effects of age on enzyme-histochemical fibre spectra and contractile properties of fast- and slow-twitch skeletal muscles in the rat. *J Neurol Sci* **76**, 69–89.

Le Rumeur E, Winder SJ & Hubert JF (2010). Dystrophin: more than just the sum of its parts. *Biochim Biophys Acta* **1804**, 1713–1722.

Lin S, Gaschen F & Burgunder JM (1998). Utrophin is a regeneration-associated protein transiently present at the sarcolemma of regenerating skeletal-muscle fibers in dystrophin-deficient hypertrophic feline muscular dystrophy. *J Neuropathol Exp Neurol* **57**, 780–790.

Lionikas A, Smith CJ, Smith TL, Bunger L, Banks RW & Bewick GS (2013). Analyses of muscle spindles in the soleus of six inbred mouse strains. *J Anat* **223**, 289–296.

Liu J, Aoki M, Illa I, Wu C, Fardeau M, Angelini C, Serrano C, Urtizberea JA, Hentati F, Hamida MB, Bohlega S, Culper EJ, Amato AA, Bossie K, Oeltjen J, Bejaoui K, McKenna-Yasek D, Hosler BA, Schurr E, Arahata K, de Jong PJ & Brown RH, Jr (1998). Dysferlin, a novel skeletal muscle gene, is mutated in Miyoshi myopathy and limb girdle muscular dystrophy. *Nat Genet* **20**, 31–36.

Lloyd EM, Xu H, Murphy RM, Grounds MD & Pinniger GJ (2019). Dysferlin-deficiency has greater impact on function of slow muscles, compared with fast, in aged BLAJ mice. *PLoS One* **14**, e0214908.

Lowe DA, Williams BO, Thomas DD & Grange RW (2006). Molecular and cellular contractile dysfunction of dystrophic muscle from young mice. *Muscle Nerve* **34**, 92–100.

Mah JK, Korngut L, Dykeman J, Day L, Pringsheim T & Jette N (2014). A systematic review and meta-analysis on the epidemiology of Duchenne and Becker muscular dystrophy. *Neuromuscul Disord* **24**, 482–491.

Mahjneh I, Marconi G, Bushby K, Anderson LV, Tolvanen-Mahjneh H & Somer H (2001). Dysferlinopathy (LGMD2B): a 23-year follow-up study of 10 patients homozygous for the same frameshifting dysferlin mutations. *Neuromuscul Disord* **11**, 20–26.

Maier A & Mayne R (1995). Basal lamina development in chicken muscle spindles. *Dev Dyn* **202**, 284–293.

Mallouk N, Jacquemond V & Allard B (2000). Elevated subsarcolemmal Ca2+ in mdx mouse skeletal muscle fibers detected with Ca2+-activated K+ channels. *Proc Natl Acad Sci U S A* **97**, 4950–4955.

Matsuda C, Aoki M, Hayashi YK, Ho MF, Arahata K & Brown RH, Jr (1999). Dysferlin is a surface membrane-associated protein that is absent in Miyoshi myopathy. *Neurology* **53**, 1119–1122.

Matsuda C, Kiyosue K, Nishino I, Goto Y & Hayashi YK (2015). Dysferlinopathy fibroblasts are defective in plasma membrane repair. *PLoS Curr* **7**, https://doi.org/10.1371/currents.md.5865add2d766f39a0e0411d38a7ba09c.

McNeil P (2009). Membrane repair redux: redox of MG53. *Nat Cell Biol* **11**, 7–9.

Mercuri E & Muntoni F (2013). Muscular dystrophy: new challenges and review of the current clinical trials. *Curr Opin Pediatr* **25**, 701–707.

Mosqueira M, Zeiger U, Forderer M, Brinkmeier H & Fink RH (2013). Cardiac and respiratory dysfunction in Duchenne muscular dystrophy and the role of second messengers. *Med Res Rev* **33**, 1174–1213.

Nahirney PC, Dow PR & Ovalle WK (1997). Quantitative morphology of mast cells in skeletal muscle of normal and genetically dystrophic mice. *Anat Rec* **247**, 341–349.

Nahirney PC & Ovalle WK (1993). Distribution of dystrophin and neurofilament protein in muscle spindles of normal and mdx-dystrophic mice: an immunocytochemical study. *Anat Rec* **235**, 501–510.

Nemoto H, Konno S, Nakazora H, Miura H & Kurihara T (2007). Histological and immunohistological changes of the skeletal muscles in older SJL/J mice. *Eur Neurol* **57**, 19–25.

Nguyen TM, Ellis JM, Love DR, Davies KE, Gatter KC, Dickson G & Morris GE (1991). Localization of the DMDL gene-encoded dystrophin-related protein using a panel of nineteen monoclonal antibodies: presence at neuromuscular junctions, in the sarcolemma of dystrophic skeletal muscle, in vascular and other smooth muscles, and in proliferating brain cell lines. *J Cell Biol* **115**, 1695–1700.

Ohlendieck K, Ervasti JM, Matsumura K, Kahl SD, Leveille CJ & Campbell KP (1991). Dystrophin-related protein is localized to neuromuscular junctions of adult skeletal muscle. *Neuron* **7**, 499–508.

Ovalle WK & Dow PR (1986). Alterations in muscle spindle morphology in advanced stages of murine muscular dystrophy. *Anat Rec* **216**, 111–126.

Pons F, Nicholson LV, Robert A, Voit T & Leger JJ (1993). Dystrophin and dystrophin-related protein (utrophin) distribution in normal and dystrophin-deficient skeletal muscles. *Neuromuscul Disord* **3**, 507–514.

Pradhan S, Ghosh D, Srivastava NK, Kumar A, Mittal B, Pandey CM & Singh U (2006). Prednisolone in Duchenne muscular dystrophy with imminent loss of ambulation. *J Neurol* **253**, 1309–1316.

Proske U (1997). The mammalian muscle spindle. *News Physiol Sci* **12**, 37–42.

Proske U & Gandevia SC (2012). The proprioceptive senses: their roles in signaling body shape, body position and movement, and muscle force. *Physiol Rev* **92**, 1651–1697.

Proske U & Gandevia SC (2018). Kinesthetic Senses. *Compr Physiol* **8**, 1157–1183.

Proske U, Gregory JE & Morgan DL (1991). Where in the muscle spindle is the resting discharge generated? *Exp Physiol* **76**, 777–785.

Rafael JA, Sunada Y, Cole NM, Campbell KP, Faulkner JA & Chamberlain JS (1994). Prevention of dystrophic pathology in mdx mice by a truncated dystrophin isoform. *Hum Mol Gen* **3**, 1725–1733.

Ribot-Ciscar E, Trefouret S, Aimonetti JM, Attarian S, Pouget J & Roll JP (2004). Is muscle spindle proprioceptive function spared in muscular dystrophies? A muscle tendon vibration study. *Muscle Nerve* **29**, 861–866.

Robert V, Massimino ML, Tosello V, Marsault R, Cantini M, Sorrentino V & Pozzan T (2001). Alteration in calcium handling at the subcellular level in mdx myotubes. *J Biol Chem* **276**, 4647–4651.

Rosales XQ, Gastier-Foster JM, Lewis S, Vinod M, Thrush DL, Astbury C, Pyatt R, Reshmi S, Sahenk Z & Mendell JR (2010). Novel diagnostic features of dysferlinopathies. *Muscle Nerve* **42**, 14–21.

Schindelin J, Arganda-Carreras I, Frise E, Kaynig V, Longair M, Pietzsch T, Preibisch S, Rueden C, Saalfeld S, Schmid B, Tinevez JY, White DJ, Hartenstein V, Eliceiri K, Tomancak P & Cardona A (2012). Fiji: an open-source platform for biological-image analysis. *Nat Methods* **9**, 676–682.

Schofield J, Houzelstein D, Davies K, Buckingham M & Edwards YH (1993). Expression of the dystrophin-related protein (utrophin) gene during mouse embryogenesis. *Dev Dyn* **198**, 254–264.

Schroder JM, Bodden H, Hamacher A & Verres C (1989). Scanning electron microscopy of teased intrafusal muscle fibers from rat muscle spindles. *Muscle Nerve* **12**, 221–232.

Sicinski P, Geng Y, Rydercook AS, Barnard EA, Darlison MG & Barnard PJ (1989). The molecular basis of muscular dystrophy in the mdx mouse – a point mutation. *Science* **244**, 1578–1580.

Skuk D, Goulet M & Tremblay JP (2010). Preservation of muscle spindles in a 27-year-old Duchenne muscular dystrophy patient: importance for regenerative medicine strategies. *Muscle Nerve* **41**, 729–730.

Sonner MJ, Walters MC & Ladle DR (2017). Analysis of proprioceptive sensory innervation of the mouse soleus: A whole-mount muscle approach. *PLoS One* **12**, e0170751.

Steinberger M, Foller M, Vogelgesang S, Krautwald M, Landsberger M, Winkler CK, Kasch J, Fuchtbauer EM, Kuhl D, Voelkl J, Lang F & Brinkmeier H (2015). Lack of the serum- and glucocorticoid-inducible kinase SGK1 improves muscle force characteristics and attenuates fibrosis in dystrophic mdx mouse muscle. *Pflügers Archiv: Eur J Physiol* **467**, 1965–1974.

Swash M & Fox KP (1976). The pathology of the muscle spindle in Duchenne muscular dystrophy. *J Neurol Sci* **29**, 17–32.

Terrill JR, Radley-Crabb HG, Iwasaki T, Lemckert FA, Arthur PG & Grounds MD (2013). Oxidative stress and pathology in muscular dystrophies: focus on protein thiol oxidation and dysferlinopathies. *FEBS J* **280**, 4149–4164.

Tinsley J, Deconinck N, Fisher R, Kahn D, Phelps S, Gillis JM & Davies K (1998). Expression of full-length utrophin prevents muscular- dystrophy in *mdx* mice. *Nature Med* **4**, 1441–1444.

Tinsley JM, Blake DJ, Roche A, Fairbrother U, Riss J, Byth BC, Knight AE, Kendrick-Jones J, Suthers GK, Love DR, Edwards YH & Davies KE (1992). Primary structure of dystrophin-related protein. *Nature* **360**, 591–593.

Tinsley JM, Fairclough RJ, Storer R, Wilkes FJ, Potter AC, Squire SE, Powell DS, Cozzoli A, Capogrosso RF, Lambert A, Wilson FX, Wren SP, De Luca A & Davies KE (2011). Daily treatment with SMTC1100, a novel small molecule utrophin upregulator, dramatically reduces the dystrophic symptoms in the mdx mouse. *PLoS One* **6**, e19189.

Turner PR, Schultz R, Ganguly B & Steinhardt RA (1993). Proteolysis results in altered leak channel kinetics and elevated free calcium in mdx muscle. *J Mem Biol* **133**, 243–251.

Turner PR, Westwood T, Regen CM & Steinhardt RA (1988). Increased protein degradation results from elevated free calcium levels found in muscle from mdx mice. *Nature* **335**, 735–738.

Umakhanova ZR, Bardakov SN, Mavlikeev MO, Chernova ON, Magomedova RM, Akhmedova PG, Yakovlev IA, Dalgatov GD, Fedotov VP, Isaev AA & Deev RV (2017). Twenty-year clinical progression of dysferlinopathy in patients from dagestan. *Front Neurol* **8**, 77.

Vafiadaki E, Reis A, Keers S, Harrison R, Anderson LV, Raffelsberger T, Ivanova S, Hoger H, Bittner RE, Bushby K & Bashir R (2001). Cloning of the mouse dysferlin gene and genomic characterization of the SJL-Dysf mutation. *Neuroreport* **12**, 625–629.

Vandebrouck C, Martin D, Colson-Van Schoor M, Debaix H & Gailly P (2002). Involvement of TRPC in the abnormal calcium influx observed in dystrophic (mdx) mouse skeletal muscle fibers. *J Cell Biol* **158**, 1089–1096.

Waddell LB, Lemckert FA, Zheng XF, Tran J, Evesson FJ, Hawkes JM, Lek A, Street NE, Lin P, Clarke NF, Landstrom AP, Ackerman MJ, Weisleder N, Ma J, North KN & Cooper ST (2011). Dysferlin, annexin A1, and mitsugumin 53 are upregulated in muscular dystrophy and localize to longitudinal tubules of the T-system with stretch. *J Neuropathol Exp Neurol* **70**, 302–313.

Waite A, Brown SC & Blake DJ (2012). The dystrophin-glycoprotein complex in brain development and disease. *Trends Neurosci* **35**, 487–496.

Wallace GQ & McNally EM (2009). Mechanisms of muscle degeneration, regeneration, and repair in the muscular dystrophies. *Annu Rev Physiol* **71**, 37–57.
Wilkinson KA, Kloefkorn HE & Hochman S (2012). Characterization of muscle spindle afferents in the adult mouse using an *in vitro* muscle-nerve preparation. *PLoS One* **7**, e39140.
Willmann R, Possekel S, Dubach-Powell J, Meier T & Ruegg MA (2009). Mammalian animal models for Duchenne muscular dystrophy. *Neuromuscul Disord* **19**, 241–249.
Wu SX, Koshimizu Y, Feng YP, Okamoto K, Fujiyama F, Hioki H, Li YQ, Kaneko T & Mizuno N (2004). Vesicular glutamate transporter immunoreactivity in the central and peripheral endings of muscle-spindle afferents. *Brain Res* **1011**, 247–251.
Zhang Y, Wesolowski M, Karakatsani A, Witzemann V & Kröger S (2014). Formation of cholinergic synapse-like specializations at developing murine muscle spindles. *Dev Biol* **393**, 227–235.
Zhang Y, Lin S, Karakatsani A, Rüegg MA & Kröger S (2015). Differential regulation of AChR clustering in the polar and equatorial region of murine muscle spindles. *European J Neurosci* **41**, 69–78.

Additional information

Author contributions

Conception and design of the work: S.K., L.G., S.R.
Acquisition, analysis and interpretation of the data: L.G., S.R., C.H., J.S., R.E.B., H.B., S.K.

Competing interests

All authors have approved the final version of the manuscript, agree to be accountable for all aspects of the work and qualify for authorship. All authors who qualify for authorship are listed as authors. All authors declare no conflict of interest.

Funding

The work was supported by grants from the Deutsche Forschungsgemeinschaft (DFG; grant KR1039/16-1), the Friedrich-Baur-Association, and the Deutsche Gesellschaft für Muskelkranke (DGM). We are particularly grateful to the FoeFoLe program of the LMU Munich, and the Munich Centre for NeuroSciences – Brain and Mind (MCN) for their generous financial support.

Acknowledgement

We would like to thank Hansruedi Brenner and Benedikt Schoser for many helpful discussions, Martina Bürkle for expert technical assistance, Magdalena Götz for constant support and encouragement, and Edith Ribot-Ciscar, Katherine Wilkinson, Guy Bewick and Bob Banks for carefully reading and improving the manuscript. We would also like to thank the Core-Facility Bioimaging of the Biomedical Centre, in particular Andreas Thomae, for invaluable help with the confocal microscopy.

Keywords

dystrophin, dysferlin, muscle spindle, proprioception, utrophin, muscular dystrophy

Supporting information

Additional supporting information may be found online in the Supporting Information section at the end of the article.

Table 1: Mean values (frequencies in imp/sec) ± SD from BL10, utro$^{-/-}$ and DMD^{mdx} mice in response to ramp-and-hold stretches.
Table 2: Mean values (frequencies in imp/sec) ± SD from BL6, dysf$^{-/-}$ and DMD^{mdx}-dysf$^{-/-}$ mice in response to ramp-and-hold stretches
Table 3: Mean values (in impulses per 9 s) ± SD of the responses of muscle spindle afferents to all 16 sinusoidal vibrations from BL10, utro$^{-/-}$ and DMD^{mdx}-mice.
Table 4: Mean values (in impulses per 9 s) ± SD of the responses of muscle spindle afferents to all 16 sinusoidal vibrations from BL6, *dysf*$^{-/-}$ and DMD^{mdx}-*dysf*$^{-/-}$ mice.
Statistical Summary Document